Accepted manuscript doi:
10.1680/jgeot.23.00308

Accepted manuscript doi:
10.1680/jgeot.23.00308

Submitted: 19 September 2023

Published online in 'accepted manuscript' format: 10 April 2024

Manuscript title: Modified cam clay bounding surface hyper-viscoplastic model

Authors: Davood Dadras-Ajirlou*, Gustav Grimstad*, Seyed Ali Ghoreishian Amiri*, Samson Abate Degago[†,‡] and Guy Tinmouth Houlsby[§]

Affiliations: *Porelab, Department of Civil and Environmental Engineering, Norwegian University of Science and Technology (NTNU), Trondheim, Norway; [†]Department of Civil and Environmental Engineering, Norwegian University of Science and Technology (NTNU), Trondheim, Norway; [‡]Department of Legislation and Regulatory Authority, Norwegian Public Roads Administration (SVV), Trondheim, Norway and [§]Department of Engineering Science, Oxford University, UK

Corresponding author: Davood Dadras-Ajirlou, Porelab, Department of Civil and Environmental Engineering, Norwegian University of Science and Technology (NTNU), Trondheim, Norway.

E-mail: davood.dadrasajirlou@ntnu.no

Accepted manuscript doi:
10.1680/jgeot.23.00308

Abstract

Clays exhibit complex mechanical behaviour with significant viscous, nonlinear, and hysteric characteristics, beyond the prediction capacity of the well-known modified cam clay (MCC) model. This paper extends the MCC model to address these important limitations. The proposed family of models is constructed entirely within the hyperplasticity framework deduced from thermodynamic extremal principles. More specifically, the previously developed MCC hyper-viscoplastic model based on the isotache concept is extended to incorporate multiple internal variables and to capture recent loading history, hysteresis, and smooth response of the material. This is achieved by defining an inelastic free energy and an element that implements a bounding surface within hyperplasticity, resulting in pressure dependency in both reversible and irreversible processes with a unique critical state envelope, and only eight material parameters with a readily measurable viscous parameter. A kinematic hardening in the logistic differential form in stress space is derived that enables the proposed model to function effectively across a wide range of stresses. Based on this kinematic hardening rule, the current stress state acts as an asymptotic attractor for the back/shift stresses whose evolution rates are proportional to their current state.

Keywords: clays; plasticity; constitutive relations; creep; rate dependence; critical state; thermodynamics

Accepted manuscript doi:
10.1680/jgeot.23.00308

1. Introduction

The modified cam clay (MCC) model (Burland 1965, Roscoe and Burland 1968), deduced from the unified and comprehensive behavioural framework of critical state soil mechanics (CSSM) (Roscoe et al. 1958, Schofield and Wroth 1968), revolutionised the understanding of the mechanical behaviour of soil, particularly clay, by linking the compressional and shearing behaviour. Although it was originally energy-based, with the normality rule for the inelastic flow imposed by Drucker's stability postulate (Drucker 1959), the MCC model has also been re-appraised within the context of modern thermodynamics. Constitutive models lacking thermodynamic validity should not be confidently used for solving boundary value problems under various loading conditions, especially those involving unloading-reloading cycles. This is because they may spuriously generate or lose energy and subsequently violate the principle of conservation of energy. For instance, studies by Zytynski et al. (1978) and Borja et al. (1997) demonstrated that a system represented by such non-conservative models may not return to its initial state after a reversible process, due to a false generation or dissipation of energy.

Shortly after its introduction, the MCC model received a thermodynamic description (Houlsby 1981), laying the foundation for its further development in a rigorous, systematic, and energy-based manner. Notably, improvements have been made to the MCC model, such as lifting the unnecessary normality rule (Collins and Hilder 2002, Collins and Kelly 2002) while maintaining maximum dissipation. This has been done just by introducing a convex and versatile dissipation potential coupled with the current state of the material. In these extensions, the approach of thermodynamics with internal variables deduced from the extremum principles (Ziegler 1977) has been employed. The systemised version of the approach, termed "Hyperplasticity", which allows a systematic development of models from a basic version, has been presented by Houlsby and Puzrin (2006). Within the hyperplasticity framework, all components of a model are integrated into two characteristic potential functions: the force/dissipation potential defining the path-dependent/irreversible behaviour, and the free energy potential defining the path-independent /reversible behaviour.

In addition to the normality restriction, which could result in extreme dilatancy for some over-consolidated clays, the original MCC model suffers from other important limitations. Perhaps, as pointed out by its founders (Roscoe and Burland 1968), the most profound deficiency, especially when prediction of soft clay behaviour is concerned, is the lack of time concept, preventing spontaneous change of the material state with a lapse of time. Adachi and Okano (1974), Kutter and Sathialingam (1992), and Yin and Graham (1999), among others, addressed the time-independency of the MCC model using the overstress theory of Perzyna (1963, 1966), which is also based on the restrictive stability postulate of Drucker (Drucker 1959), resulting in the normality restriction. Using

the hyperplasticity approach (Houlsby and Puzrin 2006), a viscoplastic MCC model has been recently developed (Dadras-Ajirlou et al. 2022, Dadras-Ajirlou et al. 2023) that lifted the normality restriction of inelastic viscous flows while the dissipation potential is maximal and, simultaneously, the CS envelope is unique under different loading rates. In this model, the viscous effects of clay behaviour are captured via the isotache concept (Šuklje 1957, Leroueil 2006) referring to a unique relationship between the inelastic strain rate (isotache) and the current state of material. The versatility of the developed model has been enhanced by incorporating the spacing ratio (Wroth and Houlsby 1985, Collins and Hilder 2002), normally defined as the ratio of the normal consolidation pressure to the pressure at the CS (Yu 1998). This addition allowed the regulation of shearing isotaches between the contractant (wet) and the dilatant (dry) zones, separated by a unique CS envelope. The inclusion of these features through the dissipative elastoplastic coupling (Collins 2002) enabled the hyper-viscoplastic model to replicate effectively the general behaviour of clay under monotonic loading with different rates, including stress relaxation and creep. This capability has been exemplified in the simulation of the well-documented behaviour of Hong Kong Marine Deposits (HKMD) (Yin and Zhu 1999, Zhu 2000, Yin et al. 2002).

Other fundamental limitations of the MCC model and its offshoots are the abrupt stiffness degradation and the lack of memory of the recent loading history, failing to capture the hysteric behaviour during unloading-reloading cycles. Several efforts (e.g., Mróz et al. (1979), Stallebrass and Taylor (1997), Rouainia and Muir Wood (2000), Kavvadas and Amorosi (2000), Houlsby (2000), Einav and Puzrin (2003)) have been made to address these important features of clay behaviour, however without considering the time and rate effects. More recently, there has been a focus on capturing the hysteresis behaviour of clay within the context of viscoplasticity, (e.g., Kimoto et al. (2015), Maranha et al. (2016), Jiang et al. (2017), Tafili and Triantafyllidis (2020), Yuan and Whittle (2021), Shi et al. (2023), and Bathayian and Maleki (2023)). Nonetheless, despite their capabilities and sophistication, some of these advanced viscoplastic models have a large number of material parameters. This motivates further research on constitutive modelling of soil behaviour with fewer material parameters, while addressing the mentioned limitations. In this regard, hyperplasticity stands out as a promising framework due to its stringent mathematical structure, ensuring unconditional thermodynamic consistency and minimising ad-hoc assumptions.

The above-mentioned important limitations of the phenomenological models, including the MCC model and its offshoots, could stem from the crude assumption of homogenous plastic flow within the Representative Elementary Volume (REV) (Coussy 1995). This is particularly relevant for clays with complex inhomogeneous microstructure which can both cause and be influenced by the inhomogeneous plastic deformation. Mesoscopic mechanical models (Einav and Collins 2008, Houlsby 2020) suggest that the inhomogeneity of plastic deformation within REV leads to phenomena

like the Bauschinger effect and hysteresis behaviour. Collins (2005) interpreted the inhomogeneous behaviour of geomaterials within REV on the mesoscale, including clay, as a signature of the formation of a network of strong and weak force chains (Radjai et al. 1998). In such a setting, it is hypothesised that the reversible energy is locked in the weak network trapped between strong networks. The trapped reversible energy is referred to as stored inelastic energy since its release can only occur through changes in the network of force chains at the mesoscopic level, induced by reversed plastic loading at the macroscopic or continuum level.

In the hyperplasticity framework, the reversible inelastic energy is integrated into the free energy potential (Collins and Houlsby 1997, Houlsby and Puzrin 2006). Following the orthogonality principle introduced by Ziegler (1977), a crucial element of the hyperplasticity framework, the inclusion of reversible inelastic energy leads to a conservative stress quantity. This quantity is termed as the back or shift stress whose evolution in stress space is known as the kinematic hardening rule. The kinematic hardening or the back stress concept has been widely adopted as an effective phenomenological modelling tool for capturing the hysteresis behaviour and Bauschinger effect (e.g., Mróz (1967), Chaboche (1989), Puzrin and Houlsby (2001), Krabbenhøft and Krabbenhøft (2021)). Nevertheless, integrating the kinematic hardening and the back stress concept into viscoplastic models within soil mechanics comes with some important consequences.

Grimstad et al. (2020) and Dadras-Ajirlou et al. (2023) have demonstrated that incorporating back stress and related kinematic hardening under isotache viscosity for a system with a single internal variable (tantamount to single yield or dynamic surface in the context of viscoplasticity) leads to non-uniqueness of the CS envelope under different loading rates, even in triaxial stress space. A unique envelope for the CS condition is an essential paradigm in CSSM that provides a reference for the unified description of the general mechanical behaviour of soils with different densities and history. A large body of test data (e.g., Arulanandan et al. (1971), Vaid and Campanella (1977), Adachi et al. (1995), Sheahan et al. (1996), Zhu (2000), Hicher (2016), Tafili et al. (2021)) strongly supports this observation, suggesting that the CS envelope is largely independent of the rate of mechanical processes. These experimental observations align with the widely used first-order approximation of Coulomb's sliding friction at macroscale (Popova and Popov 2015), which is generally considered to be almost independent of the rate of the shearing in isothermal process with no chemical reactions. The uniqueness of the CS envelope under various loading rates should be distinguished from the more subtle matter of the uniqueness of the CS envelope under different shearing modes (Lode angle) (Dafalias and Taiebat 2013, Li and Dafalias 2015).

Moreover, based on the conventional practice of the plasticity theory, back stress may be associated with a certain elastic domain that shifts by movement of the back stress according to a kinematic hardening rule. A general obstacle in this context is the establishment of the initial position of the back stress in stress space for each material point within the boundary value problem's domain. Any viscoplastic processes, including pure creep or stress relaxation, necessitates the stress state to be situated outside the considered elastic domain (Chaboche 2008).

Introducing multiple kinematic surfaces may entail additional viscous parameters (e.g., Shi et al. (2023)). Each of these additional viscosities is associated with a specific surface. However, establishing and evaluating these extra viscous parameters through the geotechnical laboratory or in-situ tests can be challenging, and may not be feasible. For a system with a single internal variable, expressing the scalar-valued dissipation function as sums of homogeneous functions with varying degrees of homogeneity results in a non-homogeneity of the dissipation function which requires a special mathematical treatment, see Puzrin and Houlsby (2003). However, a single viscosity can be sufficient to represent the essential characteristics of the material's behaviour. In the context of the creep behaviour of clay and peat, Ziegler (1972, 1981) presents an argument that aligns with the observations and statements made by Barden (1968), who advocated for simplifying a series of viscous elements with a single element having minimal viscous parameters.

The work presented in this paper builds upon the prior research (Dadras-Ajirlou et al. 2022, Dadras-Ajirlou et al. 2023) and specifically addresses the nonlinear, smooth (gradual stiffness degradation), and viscous behaviour of clay with recent loading history effect. To achieve this, the novel concept of the bounding surface in hyperplasticity (Houlsby and Richards 2023), which differs fundamentally from the bounding surface in plasticity (e.g., Dafalias and Popov (1975), Dafalias (1986), Hashiguchi (1989)), is utilised for the first time in viscoplastic modelling using the isotache viscosity. This treatment offers a minimum number of additional material parameters with only a single viscous parameter, in line with the argument by Ziegler (1972, 1981) and Barden (1968). Specifically, the classical force, flow, and free energy potentials of the basic MCC hyper-viscoplastic model (Dadras-Ajirlou et al. 2022) are enriched with additional internal variables and mechanisms using the bounding surface concept. Subsequently, the incremental formulation, including inelastic flow and kinematic hardening, are derived. To incorporate the spacing ratio and exert control over the distribution of deviatoric isotaches in the contractant and the dilatant zones, a more generalised form for force/flow potential is developed. This generalisation is designed to ensure uniqueness of the CS envelope under various loading rates. Lastly, the paper concludes with the evaluation of the efficacy of the proposed hyper-viscoplastic model in capturing the monotonic and hysteresis time-dependent

behaviour of HKMD (Yin and Zhu 1999, Zhu 2000, Yin et al. 2002) and the recent loading history effect on the time-dependent behaviour of a saturated clay taken from an earth dam core (Hicher 2016).

For clarity, the model is constructed under the same notation as the previous work for an axisymmetric system (conventional triaxial specimen) confined to isothermal and infinitesimal strain conditions. Therefore, the total strain can be expressed as sums of volumetric $\left(\varepsilon_v = \varepsilon_a + 2\varepsilon_r\right)$ and deviatoric $\left(\varepsilon_s = 2\left(\varepsilon_a - \varepsilon_r\right)/3\right)$ strains. The corresponding work-conjugate stresses are then the spherical $\left(p = \left(\sigma_a + 2\sigma_r\right)/3\right)$ and the deviatoric $\left(q = \sigma_a - \sigma_r\right)$ stresses. The subscripts "*a*" and "*r*" refer to the axial and radial components of stress and strain. Positive values are assigned to compressive strains and stresses. In the following, the notation $\left(\bullet\right)$ denotes the time derivative, all stresses are effective stresses, and inelastic volumetric $\left(\varepsilon_v^p\right)$ and deviatoric $\left(\varepsilon_s^p\right)$ strains are adopted as the internal variable of the system. The available space does not permit an outline of the hyperplasticity framework. For a detailed description of the framework, its thermodynamic rudiments, definition of the technical terminologies, and the systematic procedure for derivation of components of a constitutive model from different potentials, such as force, flow, free energy potentials, reference is made to Houlsby and Puzrin (2006).

2. Force, flow, and free energy potentials

The classical force potential (*z*) or the dissipation function (*d*) has already been constructed based on the isotache scaling (Dadras-Ajirlou et al. 2022):

$$z = \frac{d}{n} = \frac{rp_0}{n}\left(\frac{\dot{\varepsilon}_v^p + \sqrt{\left(\dot{\varepsilon}_v^p\right)^2 + \left(M\dot{\varepsilon}_s^p\right)^2}}{2r}\right)^n \qquad (1)$$

where *M* is the frictional coefficient at the CS $\left(\dot{\varepsilon}_v^p = 0\right)$, and p_0 is the isotropic pre-consolidation pressure with the definition:

$$p_0 = p_{ref}\exp\left(\frac{\varepsilon_v^p}{\lambda - \kappa}\right) \qquad (2)$$

where p_{ref} is the value of p_0 at $\varepsilon_v^p = 0$, and λ and κ are the typical CSSM compressional and swelling indexes on the bi-logarithmic plane of the specific volume versus the spherical effective stress.

The isotache scaling in Eq. (1) is considered by scaling a reference creep power (rp_0) with the ratio of current isotache per the reference isotache (reference strain rate *r*) to the power of rate sensitivity parameter *n*. For the current isotache, a mechanism without inelastic swelling has been utilized to impose the unidirectional nature of creep, which as a rheological phenomenon is a compressive and fully dissipative process under a progressive and one-way motion. Note that due to the pure scaling operation in Eq. (1), energy always dissipates, regardless of the current state of material, or absence of the external power, leading to unending creep or relaxation. However, due to the exponential form of Eq. (2) and appropriate values for *n*, this is not a practical issue (Grimstad et al. 2021, Dadras-Ajirlou et al. 2022). Nevertheless, one can simply add an extra term similar to Eq. (1) but with $n=1$ similar to the example provided by Grimstad et al. (2021) to limit the dissipation by introducing a yielding criterion. For simplicity and practicality, this limit is not implemented in the current study.

The force potential (or dissipation function) described in Eq. (1), featuring strict convexity and a positive homogeneity degree of $n \geq 1$, characterises path-dependent/irreversible behaviour due to its positive semidefinite nature. To fully define material behaviour, path-independent/reversible behaviour must also be established. To do so, the Helmholtz free energy potential (*f*) proposed by Houlsby et al. (2005) has been utilized:

$$f = \kappa p_a \exp\left(\frac{\varepsilon_v - \varepsilon_v^p + \frac{3}{2} g \left(\varepsilon_s - \varepsilon_s^p \right)^2}{\kappa} \right) \qquad (3)$$

where *g* is dimensionless material parameters defining the elastic shear modulus, and p_a is an arbitrary reference pressure (preferably atmospheric pressure). This strictly convex Helmholtz free energy potential is particularly suitable for modelling the time-dependent behaviour of clay, such as creep or stress relaxation. Its exponential form which couples volumetric and shear strains provides a reference-independent and pressure-dependent state for the material (Dadras-Ajirlou et al. 2022). These features enable the model, with the laboratory-estimated viscous and reversible material parameters, to reasonably represent the material behaviour under the in-situ condition, with a significantly different time scale and pressure. When extending the model with the bounding surface concept, these attributes should be incorporated in the plastic part of free energy, which also influences the path-independent/reversible behaviour.

The above-mentioned features also apply to the Gibbs free energy potential, the Legendre transform of the Helmholtz free energy defined in Eq. (3). For a detailed description of the role of the Legendre transformation, refer to the appendix in Collins and Houlsby (1997) and Houlsby and Puzrin (2006). The choice between the Helmholtz and Gibbs forms of the free energy potential is influenced principally by modelling preferences. In this context, the main justification for choosing the

Helmholtz form is not only to provide an aesthetically pleasing and consistent strain-based description of the system under isothermal processes but also to simplify the construction of the plastic part of free energy as a scalar-valued function of plastic strains. As presented below, the simplest form for the plastic free energy with the same attributes as of the elastic free energy presented in Eq. (3), is an exponential function of plastic volumetric and deviatoric strains.

Now, by considering the earlier construction as the bounding condition (Eqs. (1), (2), and (3)), $N-1$ additional mechanisms (including inelastic swelling) can be incorporated by increasing the number of internal variables using the bounding surface concept (Houlsby and Richards 2023):

$$z=\frac{d}{n}=\frac{rp_0}{n}\left(\frac{\dot{\varepsilon}_{vN}^{p}+\sqrt{\sum_{i=1}^{N}\left(\left(K_i\dot{\varepsilon}_{vi}^{p}\right)^2+\left(MK_i\dot{\varepsilon}_{si}^{p}\right)^2\right)}}{2r}\right)^n \qquad (4)$$

$$p_0=p_{ref}\exp\left(\frac{\sum_{i=1}^{N}\varepsilon_{vi}^{p}}{\lambda-\kappa}\right) \qquad (5)$$

$$f=\kappa p_a\exp\left(\frac{\varepsilon_v-\sum_{i=1}^{N}\varepsilon_{vi}^{p}+\frac{3}{2}g\left(\varepsilon_s-\sum_{i=1}^{N}\varepsilon_{si}^{p}\right)^2}{\kappa}\right)+\underbrace{\sum_{i=1}^{N}\left(\frac{p_a}{k_p}\right)\exp\left(k_p\left(H_i\varepsilon_{vi}^{p}+\frac{3}{2}g_p\left(H_i\varepsilon_{si}^{p}\right)^2\right)\right)}_{f_p} \qquad (6)$$

All the parameters are the same as presented previously for Eqs. (1) and (3), except the dimensionless parameters k_p, g_p, and the weight functions K_i and H_i, chosen to be:

$$K_i=\frac{i}{N} \qquad (7)$$

$$H_i=1-\frac{i}{N} \qquad (8)$$

The parameters k_p, g_p, and weight function H_i control the storage and release of reversible inelastic energy $\left(\dot{f}_p\right)$. Notice how the bounding condition is considered at $i=N$. The force potential (Eq. (4)) is still positive semidefinite with a positive homogeneity degree of $n\geq 1$ in all variables. Moreover, the plastic part of the Helmholtz free energy $\left(f_p\right)$ is structured similarly to the elastic part to maintain the pressure dependence and the reference independence attributes, as discussed earlier. The above arrangement preserves the isotache scaling properties. Further elaborations are provided in the following and the proceeding section.

Accepted manuscript doi:
10.1680/jgeot.23.00308

To understand the implications of the recent extension, an alternative expression in stress space is presented. To do so, by following the systematic procedures, the flow potential (*w*) is first computed in terms of the spherical and deviatoric dissipative stresses. Subsequently, *w* is transformed to the *p*-*q* stress space using the ZO condition. Based on the Legendre transformation, *w* can be expressed in terms of homogenous force potential *z* with homogeneity order of *n* as (Houlsby and Puzrin 2006):

$$w = d - z = (n-1)z \qquad (9)$$

In passing, it should be also realised that $w=0$ for $n=1$ (homogeneity degree of one for *d* or *z*, $z=d$) which signifies the rate-independent bounding surface form for the hyperplastic MCC model (Houlsby 1981, Collins and Houlsby 1997). Table 1 summarises the relationships between the systematic extensions of the MCC model to the viscoplastic and bounding surface forms.

The generalised dissipative stresses (χ_i) are obtained from the derivation of the force potential with respect to the corresponding work-conjugate variables (inelastic strain rates) as:

$$\chi_{pi} = \frac{\partial z}{\partial \dot{\varepsilon}_{vi}^{p}} = \left(\frac{p_0}{2}\right)\left(\frac{nz}{rp_0}\right)^{\frac{n-1}{n}}\left(\left\langle i-(N-1)\right\rangle + \frac{K_i^2\dot{\varepsilon}_{vi}^{p}}{\sqrt{\sum_{i=1}^{N}\left(\left(K_i\dot{\varepsilon}_{vi}^{p}\right)^2+\left(MK_i\dot{\varepsilon}_{si}^{p}\right)^2\right)}}\right) \qquad (10)$$

$$\chi_{qi} = \frac{\partial z}{\partial \dot{\varepsilon}_{si}^{p}} = \left(\frac{p_0}{2}\right)\left(\frac{nz}{rp_0}\right)^{\frac{n-1}{n}}\left(\frac{\left(MK_i\right)^2\dot{\varepsilon}_{si}^{p}}{\sqrt{\sum_{i=1}^{N}\left(\left(K_i\dot{\varepsilon}_{vi}^{p}\right)^2+\left(MK_i\dot{\varepsilon}_{si}^{p}\right)^2\right)}}\right) \qquad (11)$$

where $\langle\bullet\rangle$ in Eq. (10) is the Macaulay bracket. Now by combining Eqs. (10) and (11), and applying the relation between the homogenous force and flow potentials (Eq. (9)), *w* can be found after moderate algebra as:

$$w = rp_0\left(\frac{n-1}{n}\right)\left(\frac{\chi_{pN}}{p_0}\left(\frac{\sum_{i=1}^{N}\left(\left(\frac{M\chi_{pi}}{K_i}\right)^2+\left(\frac{\chi_{qi}}{K_i}\right)^2\right)}{\left(M\chi_{pN}\right)^2}\right)\right)^{\frac{n}{n-1}} = rp_0\left(\frac{n-1}{n}\right)\left(\frac{p_{eq}}{p_0}\right)^{\frac{n}{n-1}} \qquad (12)$$

where p_{eq} is called equivalent pressure. Note that the flow potential *w* exhibits a positive homogeneity degree of *n*/(*n*-1) with respect to the dissipative stresses. This is expected based on the scaling property of Legendre-conjugate homogeneous functions (1/*n* + (*n*-1)/*n* = 1).

To apply the ZO condition and complete the transformation, *p*, *q*, and the generalised conservative stresses $(\overline{\chi_i})$ are computed by taking the derivatives of the Helmholtz free energy (Eq. (6)) with respect to the corresponding conjugate variables:

$$p = \frac{\partial f}{\partial \varepsilon_v} = p_a \exp\left(\frac{\varepsilon_v - \sum_{i=1}^{N} \varepsilon_{vi}^p + \frac{3}{2} g \left(\varepsilon_s - \sum_{i=1}^{N} \varepsilon_{si}^p \right)^2}{\kappa} \right) \qquad (13)$$

$$q = \frac{\partial f}{\partial \varepsilon_s} = 3gp\left(\varepsilon_s - \sum_{i=1}^{N} \varepsilon_{si}^p \right) \qquad (14)$$

$$\overline{\chi_{pi}} = -\frac{\partial f}{\partial \varepsilon_{vi}^p} = p - p_a H_i \exp\left(k_p \left(H_i \varepsilon_{vi}^p + \frac{3}{2} g_p \left(H_i \varepsilon_{si}^p \right)^2 \right) \right) = p - p_{bi} \qquad (15)$$

$$\overline{\chi_{qi}} = -\frac{\partial f}{\partial \varepsilon_{si}^p} = q - 3gp_{bi} H_i \varepsilon_{si}^p = q - q_{bi} \qquad (16)$$

where p_{bi} and q_{bi} are the spheric and deviatoric back stresses. Notice that $p_{bN} = q_{bN} = 0$ since $H_N = 0$. Now by imposing ZO condition:

$$\begin{cases} \overline{\chi_{pi}} = \chi_{pi} \\ \overline{\chi_{qi}} = \chi_{qi} \end{cases} \qquad (17)$$

the equivalent pressure p_{eq} in Eq. (12) can be expressed in the *p*-*q* space:

$$p_{eq} = p \left(\frac{\sum_{i=1}^{N} \left(\left(\frac{M\left(p - p_{bi}\right)}{K_i} \right)^2 + \left(\frac{\left(q - q_{bi}\right)}{K_i} \right)^2 \right)}{M^2 p^2} \right) = p\left(1 + \frac{\eta^2}{M^2} \right) \qquad (18)$$

where, by considering that $p_{bN} = q_{bN} = 0$ (since $H_i = 0$), η , the stress ratio, can be defined as:

$$\eta = \frac{\sqrt{q^2 + \sum_{i=1}^{N-1} \left(\left(\frac{M\left(p - p_{bi}\right)}{K_i} \right)^2 + \left(\frac{\left(q - q_{bi}\right)}{K_i} \right)^2 \right)}}{p} \qquad (19)$$

It can now be reasoned that under the condition of ZO, the pressure dependency emerges within all formulations. The pressure dependency feature is due to the exponential coupling of the volumetric and deviatoric strains in both elastic and inelastic parts of the Helmholtz free energy (Eq. (6)), as well as the imposition of the unidirectional nature of time-dependent behaviour clay (in a phenomenological sense based on the isotache concept) within the force potential (Eq. (4)). The latest criterion is established through two choices made at the bounding condition $\left(i = N\right)$, one in the force potential $\left(z\right)$ and the other in the inelastic part of the Helmholtz free energy $\left(f_p\right)$. The first choice enforces zero dissipation for the pure plastic swelling at the bounding condition $\left(\dot{\varepsilon}_{vN}^p + \left|\dot{\varepsilon}_{vN}^p\right| = 0\right)$, while

the second ensures zero back stress at the bounding condition $(H_N = 0)$. Based on these choices and the exponential form of the free energy, pressure remains strictly positive which is required by the isotache scaling (Dadras-Ajirlou et al. 2022).

3. Incremental formulation

The incremental formulation is derived directly from two potential functions, the free energy potential representing reversible response, and the force/dissipation potential representing irreversible response. To facilitate the implementation of the model into numerical codes by employing the common numerical integration schemes, the flow potential can be used instead of the force potential to derive the irreversible incremental response completely in terms of stress.

Based on Eqs. (13) and (14) the following time differentials can be derived to describe the evolution of *p* and *q* stresses over time:

$$\dot{p} = \frac{\partial^2 f}{\partial \varepsilon_v^2}\dot{\varepsilon}_v + \frac{\partial^2 f}{\partial \varepsilon_v \partial \varepsilon_s}\dot{\varepsilon}_s + \sum_{i=1}^{N}\left(\frac{\partial^2 f}{\partial \varepsilon_v \partial \varepsilon_{vi}^p}\dot{\varepsilon}_{vi}^p + \frac{\partial^2 f}{\partial \varepsilon_v \partial \varepsilon_{si}^p}\dot{\varepsilon}_{si}^p\right) \qquad (20)$$

$$\dot{q} = \frac{\partial^2 f}{\partial \varepsilon_s \partial \varepsilon_v}\dot{\varepsilon}_v + \frac{\partial^2 f}{\partial \varepsilon_s^2}\dot{\varepsilon}_s + \sum_{i=1}^{N}\left(\frac{\partial^2 f}{\partial \varepsilon_s \partial \varepsilon_{vi}^p}\dot{\varepsilon}_{vi}^p + \frac{\partial^2 f}{\partial \varepsilon_s \partial \varepsilon_{si}^p}\dot{\varepsilon}_{si}^p\right) \qquad (21)$$

Now since:

$$\frac{\partial^2 f}{\partial \varepsilon_v^2} = -\frac{\partial^2 f}{\partial \varepsilon_v \partial \varepsilon_{vi}^p} \qquad (22)$$

$$\frac{\partial^2 f}{\partial \varepsilon_s^2} = -\frac{\partial^2 f}{\partial \varepsilon_s \partial \varepsilon_{si}^p} \qquad (23)$$

$$\frac{\partial^2 f}{\partial \varepsilon_v \partial \varepsilon_s} = \frac{\partial^2 f}{\partial \varepsilon_s \partial \varepsilon_v} = -\frac{\partial^2 f}{\partial \varepsilon_s \partial \varepsilon_{vi}^p} = -\frac{\partial^2 f}{\partial \varepsilon_v \partial \varepsilon_{si}^p} \qquad (24)$$

the above system of differentials can be simplified as:

$$\begin{bmatrix}\dot{p}\\ \dot{q}\end{bmatrix} = \underbrace{\begin{bmatrix}\frac{\partial^2 f}{\partial \varepsilon_v^2} & \frac{\partial^2 f}{\partial \varepsilon_v \partial \varepsilon_s}\\ \frac{\partial^2 f}{\partial \varepsilon_v \partial \varepsilon_s} & \frac{\partial^2 f}{\partial \varepsilon_s^2}\end{bmatrix}}_{D^e}\begin{bmatrix}\dot{\varepsilon}_v - \sum_{i=1}^{N}\dot{\varepsilon}_{vi}^p\\ \dot{\varepsilon}_s - \sum_{i=1}^{N}\dot{\varepsilon}_{si}^p\end{bmatrix} = \begin{bmatrix}\frac{p}{\kappa} & \frac{q}{\kappa}\\ \frac{q}{\kappa} & \frac{p}{\kappa}\left(3g\kappa + \frac{q^2}{p^2}\right)\end{bmatrix}\begin{bmatrix}\dot{\varepsilon}_v - \sum_{i=1}^{N}\dot{\varepsilon}_{vi}^p\\ \dot{\varepsilon}_s - \sum_{i=1}^{N}\dot{\varepsilon}_{si}^p\end{bmatrix} \qquad (25)$$

where D^e is the elasticity tensor whose components are expressed in terms of *p* and *q* based on the definition provided in Eqs. (13) and (14).

The viscoplastic strain rates, based on the definition (Houlsby and Puzrin 2006), can be directly derived from the flow potential *w* (Eq. (12)). In this regard for the bounding viscoplastic flow, there are:

Accepted manuscript doi:
10.1680/jgeot.23.00308

$$\dot{\varepsilon}_{vN}^{p}=\frac{\partial w}{\partial \chi_{pN}}=r\left(\frac{p_{eq}}{p_0}\right)^{\frac{1}{n-1}}\left(1-\left(\frac{\eta}{M}\right)^2\right) \qquad (26)$$

$$\dot{\varepsilon}_{sN}^{p}=\frac{\partial w}{\partial \chi_{qN}}=r\left(\frac{p_{eq}}{p_0}\right)^{\frac{1}{n-1}}\left(\frac{2q}{M^2 p}\right) \qquad (27)$$

and for the other viscoplastic flows:

$$\dot{\varepsilon}_{vi}^{p}=\frac{\partial w}{\partial \chi_{pi}}=r\left(\frac{p_{eq}}{p_0}\right)^{\frac{1}{n-1}}\left(\frac{2\left(p-p_{bi}\right)}{K_i^2 p}\right) \qquad (28)$$

$$\dot{\varepsilon}_{si}^{p}=\frac{\partial w}{\partial \chi_{qi}}=r\left(\frac{p_{eq}}{p_0}\right)^{\frac{1}{n-1}}\left(\frac{2\left(q-q_{bi}\right)}{\left(MK_i\right)^2 p}\right) \qquad (29)$$

In the above equations, the ZO condition (Eq. (17)) has been applied after the derivations of *w* with respect to the corresponding conjugate dissipative stresses. η in Eq. (26) refers to the definition provided in Eq. (19) for the stress ratio in the *p*-*q* stress space.

There are also two hardening rules controlling the incremental response of the material. The isotropic hardening rule refers to the evolution of p_0 during an inelastic process, which according to Eq. (5) can be expressed as:

$$\dot{p}_0=p_0\left(\frac{\sum_{i=1}^{N}\dot{\varepsilon}_{vi}^{p}}{\lambda-\kappa}\right) \qquad (30)$$

The kinematic hardening rule can be expressed as a time differential of the back stresses p_{bi} and q_{bi} defined in Eqs. (15) and (16), respectively:

$$\begin{bmatrix}\dot{p}_{bi}\\ \dot{q}_{bi}\end{bmatrix}=\begin{bmatrix}-\frac{\partial^2 f^p}{\partial \varepsilon_{vi}^2} & -\frac{\partial^2 f^p}{\partial \varepsilon_{vi}\partial \varepsilon_{si}}\\ -\frac{\partial^2 f^p}{\partial \varepsilon_{vi}\partial \varepsilon_{si}} & -\frac{\partial^2 f^p}{\partial \varepsilon_{si}^2}\end{bmatrix}\begin{bmatrix}\dot{\varepsilon}_{vi}^{p}\\ \dot{\varepsilon}_{si}^{p}\end{bmatrix}=H_i k_p\begin{bmatrix}p_{bi} & q_{bi}\\ q_{bi} & p_{bi}\left(\frac{3g_p}{k_p}+\frac{q_{bi}^2}{p_{bi}^2}\right)\end{bmatrix}\begin{bmatrix}\dot{\varepsilon}_{vi}^{p}\\ \dot{\varepsilon}_{si}^{p}\end{bmatrix} \qquad (31)$$

in which the same properties as those expressed in Eqs. (22) to (24) has been applied for f^p. Upon replacing the viscoplastic strain rate with their definitions in Eqs. (28) and (29) in which ZO condition is imposed, the kinematic hardening rule transforms to:

$$\begin{bmatrix}\dot{p}_{bi}\\ \dot{q}_{bi}\end{bmatrix}=\frac{2H_i k_p r}{K_i p}\left(\frac{p_{eq}}{p_0}\right)^{\frac{1}{n-1}}\begin{bmatrix}p_{bi} & q_{bi}\\ q_{bi} & p_{bi}\left(\frac{3g_p}{k_p}+\frac{q_{bi}^2}{p_{bi}^2}\right)\end{bmatrix}\begin{bmatrix}p-p_{bi}\\ \frac{q-q_{bi}}{M^2}\end{bmatrix} \qquad (32)$$

Accepted manuscript doi:
10.1680/jgeot.23.00308

Eq. (32) is a system of the logistic differential equations in terms of back stresses, meaning that the *p*-*q* stress state acts as an attractor for the back stresses whose evolution over time is exponential. As a result, after sufficient deformation or elapsed time during the creep/relaxation process, the short-term memory of material in terms of the relative location of back stresses with the current stress state in stress space diminishes. At such bounding states (states with faded short-term memory), like the CS or the creep/relaxation after a long time, the response of the bounding surface model is quite similar to the previous version of the model (Dadras-Ajirlou et al. 2022). This is because based on Eq. (32), the back stresses asymptotically approach the current stress state (the stable steady state of the logistic differential equation (32)) during sustained monotonic loading resulting in both infinitesimal inelastic strain rates (Eqs. (28) and (29)) and dissipation shares for the mechanisms other than the bounding mechanism. Consequently, the properties related to these bounding states are the same as in the previous version of the model. In this regard, under a pure creep process, isotropic hardening, Eq. (30), can be understood as the evolution of the material's resistance to further compression over relatively long time, i.e., the long-term memory of the material.

It is now evident that by implementing the choices made in the previous section under the condition of ZO and arriving at the viscoplastic flows (Eqs. (26)-(29)) and the kinematic hardening rule (Eq. (32)), a unique CS envelope as a bounding condition can emerge. At the CS, where the material continuously deforms under constant stress state $\left(q = Mp\right)$, the back stresses are asymptotically attracted towards the constant stress state. In this case, according to Eq. (32), $p_{bi} \simeq p$ and $q_{bi} \simeq q$, and subsequently based on Eqs. (28), (29), and (19), $\dot{\varepsilon}_{vi}^{p} \simeq 0$, $\dot{\varepsilon}_{si}^{p} \simeq 0 \left(i \neq N\right)$, and $\eta \simeq M$, respectively. As a result, the determining internal variables at the CS are the internal variables associated with the bounding condition $\left(i = N\right)$ whose volumetric rate is asymptotically zero, with the deviatoric rate continuously evolving, according to Eqs. (26) and (27) respectively. Indeed, at the CS, the response of the bounding surface model is asymptotically equal to the response of the basic model (Dadras-Ajirlou et al. 2022).

Similarly, the response of the bounding surface model is asymptotically equal to the response of the basic model under creep process, meaning that the material properties for the creep process remain consistent with those established previously based on the time resistance concept (Janbu 1969, Janbu 1985, Vermeer and Neher 1999, Grimstad et al. 2010, Jostad and Yannie 2017). Further details are provided in the following.

Fig. 1 displays the performance of the kinematic hardening rule (Eq. (32)) during a creep process under a certain constant *p*-*q* stress state. The largest surface refers to the bounding condition, and the two small, dashed surfaces denote the two additional mechanisms incorporated into the dissipation or force potential. The corresponding viscoplastic flows are also shown in Fig. 1 where the solid grey

Accepted manuscript doi:
10.1680/jgeot.23.00308

vector is associated with the flow at the bounding condition (Eqs. (26) and (27)) and the dashed vectors correspond to the two additional mechanisms (Eqs. (28) and (29)). The solid black surface defined by Eq. (18) is always convex since it is a conic combination of the bounding and the two additional mechanisms in the forms of the MCC-type ellipsoids. The solid black vectors represent the overall viscoplastic flow as the resultant of all viscoplastic flows shown in grey colour. As observed, due to creep, the two back stresses are approaching the current *p*-*q* stress state, causing two kinematic surfaces and their corresponding viscoplastic flows to converge and eventually diminish. Consequently, the short-term memory of the material fades from Fig. 1a to Fig. 1d.

It is important to note that the kinematic and bounding surfaces depicted in Fig.1 are merely theoretical representations and are not actual components of the proposed model. The sole surface with a physical significance is the dynamic surface, shown by the solid black curve defined in Eq. (18), encompassing all back stresses. Based on Eq. (18), the kinematic surfaces can be expressed as:

$$p_{eq,i} = p\left(\left(\frac{p - p_{bi}}{K_i p}\right)^2 + \left(\frac{q - q_{bi}}{MK_i p}\right)^2\right) \qquad (33)$$

where $p_{eq,i}$ is the equivalent pressure or size of the *i*th dynamic kinematic surface that is function of distance between the current stress state and the *i*th back stress.

In the context of viscoplasticity, the kinematic surfaces shown in Fig. 1 are not necessarily always bounded by the bounding surface. In fact, due to ZO condition (Eq. 17), the bounding surface only bounds the back stresses after a sufficiently long elapsed time and reduction in rate of change of material state. For instance, as shown in Fig. 2, during reversed loading or stress relaxation immediately after fading of the short-term memory during the recent sustained loading, a large domain of the kinematic surfaces can be located outside the bounding surface (generation of a new short-term memory). This is because the distance between the current stress state and the back stress state suddenly increases. However, after sufficient lapse of time and decrease in the rate of change of stress, the back stresses are asymptotically attracted to the current stress state and subsequently to the bounding surface which always passes through the origin and current stress state (due to unidirectionality condition imposed for the bounding internal variable in the force potential, as explained at the end of preceding section).

4. Generalised force and flow potentials

In this section, the force potential defined in Eq. (4), and subsequently, the flow potential computed in Eq. (12) as the conjugate of the force potential, are generalised to incorporate the spacing ratio. This extension offers flexibility to adjust the distribution of deviatoric isotaches and enhances the model's predictions of shearing behaviour under different loading rates for different types of clays.

Continuing in line with previous works (Dadras-Ajirlou et al. 2022, Dadras-Ajirlou et al. 2023), the force potential is generalised by incorporating a transition function (*T*) and the spacing ratio (*R*) as:

$$z = \frac{d}{n} = \frac{rp_0}{n}\left(\frac{\dot{\varepsilon}_{vN}^{p} + \sqrt{\left(T\dot{\varepsilon}_{vN}^{p}\right)^2 + \left(M\dot{\varepsilon}_{sN}^{p}\right)^2 + \sum_{i=1}^{N-1}\left(\left(K_i\dot{\varepsilon}_{vi}^{p}\right)^2 + \left(MK_i\dot{\varepsilon}_{si}^{p}\right)^2\right)}}{Rr} \right)^n \qquad (34)$$

where *T* is a variant of the logistic function with the state variable *S* as a varying input:

$$T = \frac{R}{2} + \left(\frac{R}{2} - 1\right)\tanh\left(S\right) \qquad (35)$$

in which *R* is greater than one and the state variable *S* is defined as:

$$S = \left(\frac{M}{\eta}\right)^2 - \left(\frac{\eta}{M}\right)^2 \qquad (36)$$

where η is defined in Eq. (19).

S is a state variable since based on Eqs. (13)-(16), *S*, under ZO condition (Eq. (17)), is linked to the Helmholtz free energy representing the current state of the material. The state variable *S* is indeed the distance of the current state of the material from the CS emerging as a bounding condition after sustained continuous deformation (details in the preceding section). The function *T* defined in Eq. (34) is called the transition function (Dadras-Ajirlou et al. 2022) due to the property of hyperbolic tangent function (tanh) that smoothly connects the contractant $\left(M > \eta\right)$ and the dilatant $\left(\eta > M\right)$ zones, separated by the critical state line passing through the desired spacing ratio $\left(q = M\,\overline{p_{eq}}/R\right)$ shown in Fig. 3b through the evolution of η.

It should be also noted that the force potential *z* or the dissipation function *d* in Eq. (34), which quantifies the amount of dissipated energy, are positive semi-definite for any rates of internal variables, like those defined previously in Eqs. (1) and (4). In this regard, it should be also emphasised that the extreme pure delayed plastic swelling (where *p* approaches zero) is discarded in all force potentials as a possible dissipative process. With these considerations in mind, by following procedures similar to those in the previous section, the flow potential can be obtained after a moderately tedious algebra as:

$$w = rp_0\left(\frac{n-1}{n}\right)\left(\frac{p_{eq}}{p_0}\right)^{\frac{n}{n-1}} \qquad (37)$$

with the following definition for the equivalent pressure in the dissipative stress space:

$$p_{eq} = \frac{R\chi_p \sqrt{\left(M^2 - \eta_\chi^2\right) + \eta_\chi^2 \left(MT + \sqrt{M^2 + \left(T^2 - 1\right)\eta_\chi^2}\right)^2}}{T\left(M^2 - \eta_\chi^2\right) + \sqrt{\left(M^2 - \eta_\chi^2\right) + \eta_\chi^2 \left(MT + \sqrt{M^2 + \left(T^2 - 1\right)\eta_\chi^2}\right)^2}} \quad (38)$$

where η_χ is the stress ratio in the dissipative stress space:

$$\eta_\chi = \frac{\sqrt{\chi_{qN}^2 + \sum_{i=1}^{N-1}\left(\left(\frac{M\chi_{pi}}{K_i}\right)^2 + \left(\frac{\chi_{qi}}{K_i}\right)^2\right)}}{\chi_{pN}} \quad (39)$$

Notice that *T* defined in Eq. (35) is the function of current stress state (through η in Eq. (36)) causing the inelastic flow to be practically non-associated, as in the basic model (Dadras-Ajirlou et al. 2022). Fig. 3 demonstrates the effect of spacing ratio *R* on the relative location of critical space. As observed, the bounding surface (solid grey curve), which controls the CS as a bounding condition, has passed the CS at the desired relative location.

It is essential to highlight that incorporating the spacing ratio in the isotache viscoplasticty using the commonly employed approach of Collins and Hilder (2002) and Collins (2003) in plasticity, where the volumetric and shearing dissipative mechanism is scaled by a function of the pre-consolidation pressure $\left(p_0\right)$, results in the loss of uniqueness of the CS envelope under different loading rates. This has been demonstrated by Grimstad et al. (2020), Grimstad et al. (2021), and Dadras-Ajirlou et al. (2023).

5. Model parameters

The proposed hyper-viscoplastic model has eight dimensionless material parameters, as detailed in Table 2. In comparison to the previous version of the model (Dadras-Ajirlou et al. 2022), only two additional parameters are introduced to control the kinematic hardening and capture hysteresis behaviour. These parameters can readily be determined through conventional triaxial, oedometer, or isotropic compression tests.

The rate sensitivity parameter (*n*) and a reference strain rate (reference isotache *r*), as mentioned previously, control the isotache scaling of a reference power $\left(rp_0\right)$. Following the approach of Grimstad et al. (2010) and Jostad and Yannie (2017), among others, *n* is defined as:

$$n = 1 + \frac{\mu}{\lambda - \kappa} \quad (40)$$

Accepted manuscript doi:
10.1680/jgeot.23.00308

where μ is the creep index. Based on the previous discussion, since the creep process occurs exclusively at the bounding condition, μ should be evaluated from a creep test. In this regard, Jostad and Yannie (2017), among others, presented a clear procedure for estimation of μ based on the time resistance concept in which $1/\mu$ is the slope of creep response in terms of strain rate against the elapsed time.

r is the average volumetric strain rate under the creep process at a certain stress ratio. It can be estimated from conventional 24-hour incremental loading oedometer or isotropic compression tests. For instance, the creep strain rate under the sustained K_0 stress state in the oedometer test, where the short-term memory has been faded, can be computed as:

$$\dot{\varepsilon}_v^p\Big|_{oed} = \dot{\varepsilon}_{vN}^p\Big|_{K_0} = \frac{\partial w}{\partial \chi_{pN}}\bigg|_{K_0} = r\left(\frac{p_{eq}}{p_0}\right)^{\frac{1}{n-1}} \frac{\partial p_{eq}}{\partial \chi_{pN}}\bigg|_{K_0} \qquad (41)$$

The creep strain rate under K_0 stress state, based on Bjerrum's equivalent time concept (Bjerrum 1967), can be defined as (Jostad and Yannie 2017):

$$\dot{\varepsilon}_v^p\Big|_{oed} = \frac{\mu}{\tau} \qquad (42)$$

where τ is the equivalent time normally equal to 24 hours. Now by assuming $p_{eq} = p_0$ after 24 hours K_0 compression, the reference isotache (*r*) can be computed by combining Eqs. (41) and (42) as:

$$r = \frac{\mu}{\tau \dfrac{\partial p_{eq}}{\partial \chi_{pN}}\Big|_{K_0}} \qquad (43)$$

Note that in Eq. (43), the derivative is first taken with respect to the spherical dissipative stress associated with the bounding condition $\left(\chi_{pN}\right)$. Then the K_0 stress state is applied by imposing the ZO condition:

$$\eta_{K_0} = \frac{\chi_{qN}}{\chi_{pN}} = \frac{q}{p} = \frac{3\left(1-K_0\right)}{1+2K_0} \qquad (44)$$

where K_0 is the radial to the axial stress ratio under sustained oedometric loading estimated by the model, not the oedometer test. To incorporate a material representative value for K_0, the proposed model can be enriched with an extra degree of freedom as practised by Collins and Hilder (2002) and Rollo and Amorosi (2020), among others.

Accepted manuscript doi:
10.1680/jgeot.23.00308

k_p and g_p, as mentioned earlier, control the performance of the kinematic hardening rule. Since kinematic hardening rule plays a crucial role in determining the reversible response through the release and storage of inelastic free energy (hysteresis), k_p and g_p should be calibrated alongside their counterparts, κ and g, which govern the release and storage of the elastic free energy. In the best scenario, k_p and κ can be first calibrated based on an isotropic hysteresis response, and then g_p and g are calibrated for a shear hysteresis response. This calibration process has been employed for the HKMD since both isotropic and shear hysteresis responses were available. It's also important to highlight that in the bounding surface form, unlike the multi-surface form (e.g., Puzrin and Houlsby (2001, 2003), Einav and Puzrin (2004), and Apriadi et al. (2013)), all dissipative mechanisms are coupled. They are neither mutually exclusive nor sequential. As a result, the number of internal variables considered significantly influences the values of k_p and g_p. Based on the authors' experience, between five to ten numbers of internal variables are sufficient for effectively capturing nonlinear and hysteresis behaviour, even for very small loading cycles. Potentially, even smaller numbers of internal variables may be sufficient if kinematic hardening moduli associated with a certain internal variable (or back stress) are discreetly calibrated (no use of weight functions), as shown by Houlsby and Richard (2023). This will remain to be explored further in future endeavours.

6. Evaluation of model

In this section, the efficacy of the proposed model in simulating the response of the reconstituted HKMD (Yin and Zhu 1999, Zhu 2000, Yin et al. 2002) and a saturated compacted clay (Hicher 2016) under different loading conditions is explored. The model parameters for these clayey soils are presented in Table 2.

The first test to consider is the 24-hour isotropic consolidation test on HKMD which includes an unloading-reloading cycle. Based on this test, which is completely uncoupled from the shear behaviour, the parameters k_p and κ are calibrated as those presented in Table 2. As shown in Fig. 4, the model response can reasonably capture the discrete experimental response, including the unloading-reloading cycle.

Next, to calibrate the parameters g_p, g, and *R*, a shearing test with loading and unloading cycles is simulated. The available test for HKMD is an undrained triaxial test with complex loading stages detailed in Table 3. Fig. 5 shows the comparison with the test data and their simulation using the calibrated parameters. Despite minor differences from the lab data, the overall performance of the model is remarkable, especially for the unloading-reloading responses which are challenging to capture.

Accepted manuscript doi:
10.1680/jgeot.23.00308

Now, to evaluate the performance of the proposed model across different stress level, the responses of a set of undrained triaxial with different initial conditions are predicted. These tests have been conducted on samples with different over-consolidation ratios $\left(OCR = p_{\max} / p\right)$. Following the original report (Zhu 2000), to construct the history of material and achieve the desired OCRs before the undrained triaxial shearing, the isotropic loading and unloading stages, both under 36 hours, are first performed. Fig. 6 displays the comparison between the measured and predicted responses. As can be observed, the model can function under different initial stress states before shearing, thanks to the logistic differential form of the kinematic hardening rule (Eq. (32)). Considering the challenge of capturing the behaviour of HKMD as shown in earlier attempts (Yin et al. (2002), Bodas Freitas et al. (2011), Islam and Gnanendran (2017), Yang et al. (2016), Shahbodagh et al. (2020), Mánica et al. (2021), Yao et al. (2015), Qiao et al. (2016), and Bathayian and Maleki (2023)), the overall performance of the model in both rate- dependent monotonic and hysteresis behaviour of HKMD is reasonably good.

To assess the proposed model's effectiveness in capturing the effects of recent loading, simulations are extended using the tests conducted by Hicher (2016) on a saturated compacted clay from an earth dam core at a depth between 5 and 8 m. This experimental study is unusual and provides insights into the influence of recent loading history on the creep and stress relaxation behaviour of clay. The measurable parameters of the model in Table 2 are selected based on the values reported by Li et al. (2022) and Shi et al. (2023).

The first sets of tests to consider are the undrained triaxial tests under various loading rates. The comparison between the test and simulation results is illustrated in Fig 7. Fig. 8 shows the comparison for creep test under axisymmetric undrained condition at different deviatoric stress level obtained under strain rate of 1%/min. These results indicate the capability of the model in capturing the conventional rate and creep behaviour of the saturated compacted clay based on selected values for parameters, particularly the single viscous parameter (μ).

The results of the undrained triaxial test, showing the effects of recent loading history on the time-dependent behaviour, are compared with the simulation results in Fig. 9. This test, conducted at strain rate of 1%/min, includes two unloading-reloading cycles with nine stress relaxation phases (represented by markers SR 1 to 9) conducted at various stages of the loading, unloading, and reloading processes. Notably, after each loading-unloading cycle, the difference between the test results and simulation in the loading processes increases. Interestingly, the test exhibits a stiffer response than the simulation, even for strains below 2%, contrary to the triaxial test under the same conditions in Fig. 7, where the simulation shows a stiffer response, particularly for strains below 2%.

The detailed effect of recent loading history on relaxation behaviour, in terms of deviatoric stress increment, is depicted for each phase in Fig. 10. The relaxation immediately after loading at phases SR 1, SR 3, and SR 7 resulted in a decrease in deviatoric stress in both the test and simulation results. In contrast, immediately after unloading at phases SR 2 and SR 9, deviatoric stress increases in both the test and simulation. Interestingly, at intermediate stages of the unloading and reloading processes, specifically at phases SR 5 and SR 6, the relaxation in both the test and simulation exhibits an opposite response compared to those occurring at SR 3 and SR 2, respectively, which occurred at the initial stages of the unloading and reloading processes. Particularly noteworthy are the relaxation phases SR 4 and SR 8, where the model was less successful in capturing the response. In these phases, occurring after stress decrease due to relaxation in phases SR 3 and SR 7 followed by slight unloading (0.1% decrease of axial strain), deviatoric stress initially increases and then decreases. The model can capture this particular behaviour to some extent for phase SR 8, but for phase SR 4, it is unsuccessful. However, overall, the model performs reasonably well in capturing hysteresis, rate, and time-dependent behaviour with the recent loading history effect, especially when compared to the limited attempts in the literature (Li et al. 2022, Shi et al. 2023) to predict the challenging behaviour of this clay (Hicher 2016) under complex loading conditions.

7. Conclusion

This study has extended the previously developed hyper-viscoplastic model (Dadras-Ajirlou et al. 2022) by incorporating inelastic free energy and the bounding surface concept (Houlsby and Richards 2023) to capture the nonlinear and hysteresis behaviour of clay. The models are mathematically rigor and are guaranteed to obey the laws of thermodynamics since they have been built entirely within the hyperplasticity framework (Houlsby and Puzrin 2006) by specifying two potential functions, one for reversible and the other for irreversible behaviour. In addition, the proposed model with inelastic free energy complies with the critical state soil mechanics (CSSM) and the isotache concept. As a result, the main limitation of the basic hyper-viscoplastic model (Dadras-Ajirlou et al. 2022, Dadras-Ajirlou et al. 2023), namely the discard of inelastic free energy for securing a unique critical state (CS) envelope, has been lifted. Another salient feature of the model is the pressure dependency (a common feature of geomaterials behaviour) in both reversible and irreversible behaviour. There are overall eight dimensionless material parameters in the proposed model. Three of these parameters pertain to the bounding conditions of the pure creep and the CS and can be straightforwardly measured from the conventional laboratory tests. While some of the other five parameters can be estimated from laboratory tests, it is recommended to calibrate them collectively against the conventional undrained triaxial, oedometer or isotropic compression tests with at least a cycle of unloading and reloading. The efficacy of the model in capturing the hysteresis and the effect of recent loading history on the time-

dependent behaviour of clays has been demonstrated by simulating a set of laboratory tests on the reconstituted Hong Kong Marine Deposits (Yin and Zhu 1999, Zhu 2000, Yin et al. 2002) and a saturated compacted clay (Hicher 2016).

Clearly, the ultimate goal of any constitutive model is its application in solving engineering boundary value problems. To this end, the numerical integration of the incremental formulation over strain and time increments is crucial. Based on the simple incremental formulation of the proposed model, the most commonly used algorithms, such as explicit modified-forward Euler with error control (Sloan 1987) or implicit backward Euler (e.g., Simo and Hughes (1998) and Heeres et al. (2002)), can be employed for the numerical integration. In fact, their application in the integration of the proposed model is straightforward because of deliberate omission of the yield criterion for pragmatic reasons. In addition to these conventional algorithms, integration of the model can be undertaken directly from the hyperplasticity relationships, rather the incremental formulation, as shown by Ghoreishian Amiri et al. (2023).

Acknowledgement

This paper was motivated by general studies of the mechanical behaviour of soft natural soils in a research project named SAUNA (SAfety of Urbanised NAtural slopes). SAUNA is an industry-academic collaboration project on the safety assessment of natural slopes in Norway and is sponsored by the Norwegian Public Roads Administration (SVV), the Norwegian Water Resources and Energy Directorate (NVE), Bane NOR, and the Norwegian University of Science and Technology (NTNU). This work was also supported by the Research Council of Norway through its Centres of Excellence funding scheme, Grant Number 262644- Porelab. All support is sincerely acknowledged. Any opinions, findings, conclusions, or recommendations expressed in this paper are those of the authors and do not necessarily reflect the views of the SAUNA Project collaborators or the Research Council of Norway. Special gratitude goes to Arnstein Watn, Prof. Steinar Nordal, and Prof. Gudmund Reidar Eiksund, for their contributions in enabling this research.

Notations

d	Scalar valued dissipation function
f	Helmholtz free energy potential
g	Dimensionless coefficient for elastic shear modulus
H_i	Weight function
K_i	Weight function
g_p	Dimensionless coefficient for kinematic hardening modulus
k_p	Dimensionless kinematic coefficient for hardening modulus
M	Slope of critical state line in p-q stress space
n	Rate sensitivity parameter (dimensionless)
OCR	Over consolidation ratio
p	Mean effective pressure
p_0	isotropic pre-consolidation pressure
p_a	Reference pressure (atmospheric pressure)

p_b	Spherical back stress
p_{eq}	Equivalent pressure
q	Deviatoric stress invariant
q_b	Deviatoric back stress
R	Spacing ratio
r	Arbitrary reference strain rate
S	State variable
T	Transition function
w	Flow potential
z	Force potential
$\varepsilon_s, \varepsilon_s^p$	Total and plastic deviatoric strains
$\varepsilon_v, \varepsilon_v^p$	Total and plastic volumetric strains
η	Stress ratio in *p*-*q* stress space
η_χ	Stress ratio in dissipative stress space
κ	Swelling index
λ	Compression index
μ	Creep index
τ	Arbitrary reference equivalent time (normally 24 hrs.)
χ_p, χ_q	Spherical and deviatoric dissipative stresses

References

Adachi, T., F. Oka, T. Hirata, T. Hashimoto, J. Nagaya, M. Mimura and T. B. S. Pradhan (1995). "Stress-strain behavior and yielding characteristics of eastern Osaka clay." SOILS AND FOUNDATIONS 35(3): 1-13.

Adachi, T. and M. Okano (1974). "A Constitutive Equation for Normally Consolidated Clay." Soils and Foundations 14(4): 55-73.

Apriadi, D., S. Likitlersuang and T. Pipatpongsa (2013). "Loading path dependence and non-linear stiffness at small strain using rate-dependent multisurface hyperplasticity model." Computers and Geotechnics 49: 100-110.

Arulanandan, K., C. K. Shen and R. B. Young (1971). "Undrained Creep Behaviour of a Coastal Organic Silty Clay." Géotechnique 21(4): 359-375.

Barden, L. (1968). "Primary and Secondary Conslidation of Clay and Peat." Géotechnique 18(1): 1-24.

Bathayian, S. M. H. and M. Maleki (2023). "Kinematic hardening based coupled elastoplastic–viscoplastic model for describing time-dependent behavior of soils subjected to non-monotonic loadings." Computers and Geotechnics 161: 105602.

Bjerrum, L. (1967). "Engineering Geology of Norwegian Normally-Consolidated Marine Clays as Related to Settlements of Buildings." Géotechnique 17(2): 83-118.

Bodas Freitas, T. M., D. M. Potts and L. Zdravkovic (2011). "A time dependent constitutive model for soils with isotach viscosity." Computers and Geotechnics 38(6): 809-820.

Borja, R. I., C. Tamagnini and A. Amorosi (1997). "Coupling Plasticity and Energy-Conserving Elasticity Models for Clays." Journal of Geotechnical and Geoenvironmental Engineering 123(10): 948-957.

Burland, J. B. (1965). "The yielding and dilation of clay." Géotechnique 15(2): 211-214.

Chaboche, J. L. (1989). "Constitutive equations for cyclic plasticity and cyclic viscoplasticity." International Journal of Plasticity 5(3): 247-302.

Chaboche, J. L. (2008). "A review of some plasticity and viscoplasticity constitutive theories." International Journal of Plasticity 24(10): 1642-1693.

Collins, I. F. (2002). "Associated and Non-Associated Aspects of the Constitutive Laws for Coupled Elastic/Plastic Materials." International Journal of Geomechanics 2(2): 259-267.

Collins, I. F. (2003). "A systematic procedure for constructing critical state models in three dimensions." International Journal of Solids and Structures 40(17): 4379-4397.

Collins, I. F. (2005). "The concept of stored plastic work or frozen elastic energy in soil mechanics." Géotechnique 55(5): 373-382.

Collins, I. F. and T. Hilder (2002). "A theoretical framework for constructing elastic/plastic constitutive models of triaxial tests." International Journal for Numerical and Analytical Methods in Geomechanics 26(13): 1313-1347.

Collins, I. F. and G. T. Houlsby (1997). "Application of thermomechanical principles to the modelling of geotechnical materials." Proceedings of the Royal Society of London. Series A: Mathematical, Physical and Engineering Sciences 453(1964): 1975-2001.

Collins, I. F. and P. A. Kelly (2002). "A thermomechanical analysis of a family of soil models." Géotechnique 52(7): 507-518.

Coussy, O. (1995). Mechanics of porous continua. Chichester, Wiley.

Dadras-Ajirlou, D., G. Grimstad and S. Ali Ghoreishian Amiri (2022). "On the isotache viscous modelling of clay behaviour using the hyperplasticity approach." Géotechnique.

Dadras-Ajirlou, D., G. Grimstad, S. Ali Ghoreishian Amiri and S. Nordal (2023). "A set of hyper-viscoplastic critical state models with different friction mobilisation criteria." International Journal of Solids and Structures 273: 112267.

Dafalias, Y. F. (1986). "Bounding Surface Plasticity. I: Mathematical Foundation and Hypoplasticity." Journal of Engineering Mechanics 112(9): 966-987.

Dafalias, Y. F. and E. P. Popov (1975). "A model of nonlinearly hardening materials for complex loading." Acta Mechanica 21(3): 173-192.

Dafalias, Y. F. and M. Taiebat (2013). "Anatomy of rotational hardening in clay plasticity." Géotechnique 63(16): 1406-1418.

Drucker, D. C. (1959). "A Definition of Stable Inelastic Material." Journal of Applied Mechanics 26(1): 101-106.

Einav, I. and I. F. Collins (2008). "A thermomechanical framework of plasticity based on probabilistic micromechanics." Journal of Mechanics of Materials and Structures 3(5): 867-892.

Einav, I. and A. M. Puzrin (2003). "Evaluation of continuous hyperplastic critical state (CHCS) model." Géotechnique 53(10): 901-913.

Einav, I. and A. M. Puzrin (2004). "Continuous hyperplastic critical state (CHCS) model: Derivation." International Journal of Solids and Structures 41(1): 199-226.

Ghoreishian Amiri, S. A., D. Dadras-Ajirlou and G. Grimstad (2023). Direct integration method for hyperplastic models. 10th European Conference on Numerical Methods in Geotechnical Engineering L. Zdravkovic, S. Kontoe, D. Taborda and A. Tsiampousi. London, UK.

Grimstad, G., D. Dadras-Ajirlou and S. A. G. Amiri (2020). "Modelling creep in clay using the framework of hyper-viscoplasticity." Géotechnique Letters 10(3): 404-408.

Grimstad, G., S. A. Degago, S. Nordal and M. Karstunen (2010). "Modeling creep and rate effects in structured anisotropic soft clays." Acta Geotechnica 5(1): 69-81.

Grimstad, G., M. Long, D. Dadras-Ajirlou and S. A. G. Amiri (2021). "Investigation of Development of the Earth Pressure Coefficient at Rest in Clay During Creep in the Framework of Hyper-Viscoplasticity." International Journal of Geomechanics 21(1): 04020235.

Hashiguchi, K. (1989). "Subloading surface model in unconventional plasticity." International Journal of Solids and Structures 25(8): 917-945.

Heeres, O. M., A. S. J. Suiker and R. de Borst (2002). "A comparison between the Perzyna viscoplastic model and the Consistency viscoplastic model." European Journal of Mechanics - A/Solids 21(1): 1-12.

Hicher, P. Y. (2016). "Experimental study of viscoplastic mechanisms in clay under complex loading." Géotechnique 66(8): 661-669.

Houlsby, G. T. (1981). Study of plasticity theories and their applicability to soils PhD Thesis, University of Cambridge.

Houlsby, G. T. (2000). Critical state models and small-strain stiffness. Developments in Theoretical Geomechanics. Proceedings of the Booker Memorial Symposium, Sydney, N.S.W., Rotterdam, Netherlands; Brookfiels, VT : A.A. Balkema.

Houlsby, G. T. (2020). Hyperplasticity: From Micro to Macro. Views on Microstructures in Granular Materials. P. Giovine, P. M. Mariano and G. Mortara. Cham, Springer International Publishing: 87-106.

Houlsby, G. T., A. Amorosi and E. Rojas (2005). "Elastic moduli of soils dependent on pressure: a hyperelastic formulation." Géotechnique 55(5): 383-392.

Houlsby, G. T. and A. M. Puzrin (2006). Principles of Hyperplasticity: an Approach to Plasticity Theory Based on Thermodynamic Principles. London, Springer

Houlsby, G. T. and I. A. Richards (2023). "Multi-surface and bounding surface models in hyperplasticity." Computers and Geotechnics 156: 105143.

Islam, M. N. and C. T. Gnanendran (2017). "Elastic-Viscoplastic Model for Clays: Development, Validation, and Application." Journal of Engineering Mechanics 143(10): 04017121.

Janbu, N. (1969). The resistance concept applied to deformations of soils. Proceedings of the 7th international conference on soil mechanics and foundation engineering, Mexico city.

Janbu, N. (1985). "Soil models in offshore engineering." Géotechnique 35(3): 241-281.

Jiang, J., H. I. Ling, V. N. Kaliakin, X. Zeng and C. Hung (2017). "Evaluation of an anisotropic elastoplastic–viscoplastic bounding surface model for clays." Acta Geotechnica 12(2): 335-348.

Jostad, H. P. and J. Yannie (2017). "A procedure for determining long-term creep rates of soft clays by triaxial testing." European Journal of Environmental and Civil Engineering 26(7): 2600-2615.

Kavvadas, M. and A. Amorosi (2000). "A constitutive model for structured soils." Géotechnique 50(3): 263-273.

Kimoto, S., B. S. Khan, M. Mirjalili and F. Oka (2015). "Cyclic Elastoviscoplastic Constitutive Model for Clay Considering Nonlinear Kinematic Hardening Rules and Structural Degradation." International Journal of Geomechanics 15(5): A4014005.

Krabbenhøft, K. and J. Krabbenhøft (2021). "Simplified kinematic hardening plasticity framework for constitutive modelling of soils." Computers and Geotechnics 138: 104146.

Kutter, B. L. and N. Sathialingam (1992). "Elastic-viscoplastic modelling of the rate-dependent behaviour of clays." Géotechnique 42(3): 427-441.

Leroueil, S. (2006). The isotache approach. Where are we 50 years after its development by Professor Šuklje? (2006 Prof. Šuklje's Memorial Lecture). Proceedings of the 13th Danube European conference on geotechnical engineering, Ljubljana, Slovenia, Slovenian Geotechnical Society.

Li, J., D.-M. Zhang, P.-Y. Hicher and C.-F. Wei (2022). "Three-dimensional modelling of stress relaxation of soft clay under complex loading conditions." European Journal of Environmental and Civil Engineering 26(7): 2496-2508.

Li, X. S. and Y. F. Dafalias (2015). "Dissipation consistent fabric tensor definition from DEM to continuum for granular media." Journal of the Mechanics and Physics of Solids 78: 141-153.

Mánica, M. A., A. Gens, E. Ovando-Shelley, E. Botero and J. Vaunat (2021). "An effective combined framework for modelling the time-dependent behaviour of soft structured clays." Acta Geotechnica 16(2): 535-550.

Maranha, J. R., C. Pereira and A. Vieira (2016). "A viscoplastic subloading soil model for rate-dependent cyclic anisotropic structured behaviour." International Journal for Numerical and Analytical Methods in Geomechanics 40(11): 1531-1555.

Mróz, Z. (1967). "On the description of anisotropic workhardening." Journal of the Mechanics and Physics of Solids 15(3): 163-175.

Mróz, Z., V. A. Norris and O. C. Zienkiewicz (1979). "Application of an anisotropic hardening model in the analysis of elasto–plastic deformation of soils." Géotechnique 29(1): 1-34.

Perzyna, P. (1963). "The constitutive equations for rate sensitive plastic materials." Quarterly of applied mathematics 20(4): 321-332.

Perzyna, P. (1966). Fundamental Problems in Viscoplasticity. Advances in Applied Mechanics. G. G. Chernyi, H. L. Dryden, P. Germain et al., Elsevier. 9: 243-377.

Popova, E. and V. L. Popov (2015). "The research works of Coulomb and Amontons and generalized laws of friction." Friction 3(2): 183-190.

Puzrin, A. M. and G. T. Houlsby (2001). "Fundamentals of kinematic hardening hyperplasticity." International Journal of Solids and Structures 38(21): 3771-3794.

Puzrin, A. M. and G. T. Houlsby (2003). "Rate-Dependent Hyperplasticity with Internal Functions." Journal of Engineering Mechanics 129(3): 252-263.

Qiao, Y., A. Ferrari, L. Laloui and W. Ding (2016). "Nonstationary flow surface theory for modeling the viscoplastic behaviors of soils." Computers and Geotechnics 76: 105-119.

Radjai, F., D. E. Wolf, M. Jean and J.-J. Moreau (1998). "Bimodal Character of Stress Transmission in Granular Packings." Physical Review Letters 80(1): 61-64.

Rollo, F. and A. Amorosi (2020). "SANICLAY-T: Simple thermodynamic-based anisotropic plasticity model for clays." Computers and Geotechnics 127: 103770.

Roscoe, K. H. and J. B. Burland (1968). On the generalized stress-strain behaviour of wet clay. Engineering Plasticity, Cambridge, Cambridge University Press, New York.

Roscoe, K. H., A. N. Schofield and C. P. Wroth (1958). "On The Yielding of Soils." Géotechnique 8(1): 22-53.

Rouainia, M. and D. Muir Wood (2000). "A kinematic hardening constitutive model for natural clays with loss of structure." Géotechnique 50(2): 153-164.

Schofield, A. N. and C. P. Wroth (1968). Critical State Soil Mechanics. New York, McGraw-Hill

Shahbodagh, B., T. N. Mac, G. A. Esgandani and N. Khalili (2020). "A Bounding Surface Viscoplasticity Model for Time-Dependent Behavior of Soils Including Primary and Tertiary Creep." International Journal of Geomechanics 20(9): 04020143.

Sheahan, T. C., C. C. Ladd and J. T. Germaine (1996). "Rate-Dependent Undrained Shear Behavior of Saturated Clay." Journal of Geotechnical Engineering 122(2): 99-108.

Shi, Z., D. Muir Wood, M. Huang and J. P. Hambleton (2023). "Tay creep: a multi-mechanism model for rate-dependent deformation of soils." Géotechnique 73(4): 310-322.

Simo, J. C. and T. J. Hughes (1998). Computational inelasticity, Springer Science & Business Media.

Sloan, S. W. (1987). "Substepping schemes for the numerical integration of elastoplastic stress–strain relations." International Journal for Numerical Methods in Engineering 24(5): 893-911.

Stallebrass, S. E. and R. N. Taylor (1997). "The development and evaluation of a constitutive model for the prediction of ground movements in overconsolidated clay." Géotechnique 47(2): 235-253.

Šuklje, L. (1957). The analysis of the consolidation process by the isotache method. Proceedings of the 4th International Conference on Soil Mechanics and Foundation Engineering, London, UK.

Tafili, M. and T. Triantafyllidis (2020). "AVISA: anisotropic visco-ISA model and its performance at cyclic loading." Acta Geotechnica 15(9): 2395-2413.

Tafili, M., T. Wichtmann and T. Triantafyllidis (2021). "Experimental investigation and constitutive modeling of the behaviour of highly plastic Lower Rhine clay under monotonic and cyclic loading." Canadian Geotechnical Journal 58(9): 1396-1410.

Vaid, Y. P. and R. G. Campanella (1977). "Time-Dependent Behavior of Undisturbed Clay." Journal of the Geotechnical Engineering Division 103(7): 693-709.

Vermeer, P. and H. Neher (1999). A soft soil model that accounts for creep. Beyond 2000 in computational geotechnics. R. B. J. Brinkgreve, Routledge: 249-261.

Wroth, C. P. and G. T. Houlsby (1985). Soil mechanics-property characterization and analysis procedures. 11th International Conference on Soil Mechanics and Foundation Engineering. San Francisco, USA: 1-55.

Yang, C., J. P. Carter, D. Sheng and S. W. Sloan (2016). "An isotach elastoplastic constitutive model for natural soft clays." Computers and Geotechnics 77: 134-155.

Yao, Y.-P., L.-M. Kong, A.-N. Zhou and J.-H. Yin (2015). "Time-Dependent Unified Hardening Model: Three-Dimensional Elastoviscoplastic Constitutive Model for Clays." Journal of Engineering Mechanics 141(6): 04014162.

Yin, J.-H. and J. Graham (1999). "Elastic viscoplastic modelling of the time-dependent stress-strain behaviour of soils." Canadian Geotechnical Journal 36(4): 736-745.

Yin, J.-H. and J.-G. Zhu (1999). "Measured and predicted time-dependent stress-strain behaviour of Hong Kong marine deposits." Canadian Geotechnical Journal 36(4): 760-766.

Yin, J.-H., J.-G. Zhu and J. Graham (2002). "A new elastic viscoplastic model for time-dependent behaviour of normally and overconsolidated clays: theory and verification." Canadian Geotechnical Journal 39(1): 157-173.

Yu, H. S. (1998). "CASM: a unified state parameter model for clay and sand." International Journal for Numerical and Analytical Methods in Geomechanics 22(8): 621-653.

Yuan, Y. and A. J. Whittle (2021). "Formulation of a new elastoviscoplastic model for time-dependent behavior of clay." International Journal for Numerical and Analytical Methods in Geomechanics 45(6): 843-864.

Zhu, J. G. (2000). Experimental study and elastic visco-plastic modelling of the time-dependent stress-strain behaviour of Hong Kong marine deposits PhD Thesis, Hong Kong Polytechnic University.

Ziegler, H. (1972). "Systems with internal parameters obeying the orthogonality condition." Zeitschrift für angewandte Mathematik und Physik ZAMP 23(4): 553-566.

Ziegler, H. (1977). An Introduction to Thermodynamics. Amsterdam, North-Holland

Ziegler, H. (1981). “Discussion of some objections to thermomechanical orthogonality.” Ingenieur-Archiv 50(3): 149-164.

Zytynski, M., M. F. Randolph, R. Nova and C. P. Wroth (1978). “On modelling the unloading-reloading behaviour of soils.” International Journal for Numerical and Analytical Methods in Geomechanics 2(1): 87-93.

Table 1. Summary of potential functions defining different version of the MCC model

Model version	Free energy potential	Force potential
Hyper-plastic MCC (equivalent to viscoplastic with $n=1$)	$f=\kappa p_a \exp\left(\frac{\varepsilon_v-\varepsilon_v^p+\frac{3}{2}g\left(\varepsilon_s-\varepsilon_s^p\right)^2}{\kappa}\right)$	$z=p_0\left(\frac{\dot{\varepsilon}_v^p+\sqrt{\left(\dot{\varepsilon}_v^p\right)^2+\left(M\dot{\varepsilon}_s^p\right)^2}}{2}\right)$
Hyper-viscoplastic MCC		$z=\frac{rp_0}{n}\left(\frac{\dot{\varepsilon}_v^p+\sqrt{\left(\dot{\varepsilon}_v^p\right)^2+\left(M\dot{\varepsilon}_s^p\right)^2}}{2r}\right)^n$
Hyper-plastic bounding surface MCC (equivalent to viscoplastic with $n=1$)	$f=\kappa p_a \exp\left(\frac{\varepsilon_v-\sum_{i=1}^{N}\varepsilon_{vi}^p+\frac{3}{2}g\left(\varepsilon_s-\sum_{i=1}^{N}\varepsilon_{si}^p\right)^2}{\kappa}\right)$ $+\sum_{i=1}^{N}\left(\frac{p_a}{k_p}\right)\exp\left(k_p\left(H_i\varepsilon_{vi}^p+\frac{3}{2}g_p\left(H_i\varepsilon_{si}^p\right)^2\right)\right)$, $H_i=1-\frac{i}{N}$	$z=p_0\left(\frac{\dot{\varepsilon}_{vN}^p+\sqrt{\sum_{i=1}^{N}\left(\left(K_i\dot{\varepsilon}_{vi}^p\right)^2+\left(MK_i\dot{\varepsilon}_{si}^p\right)^2\right)}}{2}\right)$, $K_i=\frac{i}{N}$
Hyper-viscoplastic bounding surface MCC		$z=\frac{rp_0}{n}\left(\frac{\dot{\varepsilon}_{vN}^p+\sqrt{\sum_{i=1}^{N}\left(\left(K_i\dot{\varepsilon}_{vi}^p\right)^2+\left(MK_i\dot{\varepsilon}_{si}^p\right)^2\right)}}{2r}\right)^n$, $K_i=\frac{i}{N}$

Accepted manuscript doi:
10.1680/jgeot.23.00308

Table 2. Dimensionless parameters of the model and their values for HKMD and a compacted clay (CC)

Model parameters	Description		Required test	HKMD*	CC**
Calibrated parameters for N = 10 (ten numbers of internal varaibles)					
κ	Swelling index		IC or Oedometer tests with URC	0.0102	0.01
g	shear modulus coefficient		T(U) or Oedometer tests with URC	125	100
k_p	kinematic hardening coefficient		T(U) or Oedometer tests with URC	4000	700
g_p	kinematic hardening coefficient		T(U) or Oedometer tests with URC	900	350
R	Spacing ratio		T(U)	2.175	2.1
Laboratory estimated parameters					
μ	Creep index		IC or Oedometer creep tests	0.0025	0.003
λ	Compression index		IC or Oedometer tests	0.0792	0.092
M	Slope of critical state line in p-q stress space		T(U)	1.265	1.07

* The measured parameters are taken from original reports (Yin and Zhu 1999, Zhu 2000, Yin et al. 2002).
** The measured parameters are taken from Shi et al. (2023).
Abbreviations: IC, Isotropic Consolidation (IC); T(U), Triaxial (Undrained preferably); URC, Unloading Reloading Cycle

Table 3. Loading history of the multi-stage triaxial compression test on HKMD (Yin et al. 2002)

Schedule	Loading	Unloading	Reloading	Relaxation	Loading	Relaxation	Loading	Relaxation
Axial strain rate (1/min)	0.1%	−0.1%	0.1%	0	0.01%	0	0.001%	0
Duration (min)	29	7	20	2540	232	1320	830	705

Figure captions

Fig. 1. Attraction of back stresses by current stress state and erase of short-term memory during a pure creeping process a-b-c-d. Back stresses are shown by plus and asterisk signs and $M = 1.2$.

Fig. 2. Generation of new short-term memory due to the reversed loading immediately after the state shown in Fig. 1d. Note that $M = 1.2$ and back stresses shown by plus and asterisk signs are overlapping due to their attraction during the previous creeping process.

Fig. 3. Effect of the spacing ratio $R = 3$ on the bounding and kinematic surfaces during a creep process a-b with (a) short-term memory and (b) faded short-term memory. Note that $M = 1.2$, the back stresses are shown by plus and asterisk signs, and $\bar{p}_{eq}$ is the equivalent pressure of the bounding surface defined exclusively based on the current stress state (as in Dadras-Ajirlou et al. (2022)) without any back stresses.

Fig. 4. Comparison between the experimental (Yin et al. 2002) and the simulated 24 h isotropic loading and unloading test on reconstituted HKMD.

Fig. 5. Comparison between the experimental (Yin et al. 2002) and the simulated results of multi-stage undrained triaxial compression test on reconstituted and normally consolidated HKMD in terms of: (a) deviatoric stress against axial strain; (b) excess pore water pressure against axial strain; (c) deviatoric stress against mean effective stress.

Fig. 6. Comparison between the experimental (Yin et al. 2002) and the simulated undrained triaxial compression tests on reconstituted HKMD with different OCRs under constant axial strain rate of 1·5%/h in terms of (a) the stress–strain response and (b) the normalised effective stress path. Note that $p_{\max}$ is the maximum isotropic consolidation pressure, the initial stress for $OCR = 1$ is $p = 400$ kPa, and for the other OCRs is $p = 100$ kPa.

Fig. 7. Comparison between the experimental (Hicher 2016) and the simulated undrained triaxial compression tests on saturated compacted clay under different strain rates in terms of (a) deviatoric stress versus axial strain response and (b) the effective stress path in p-q stress space.

Fig. 8. Comparison between the experimental (Hicher 2016) and the simulated undrained triaxial creep tests at different deviatoric stresses obtained under strain rate of 1%/min in terms of (a) axial strain and (b) excess pore water pressure versus time.

Fig. 9. Comparison between the experimental (Hicher 2016) and the simulated undrained triaxial test under strain rate of 1%/min with two unloading-reloading cycles and nine relaxation phases (SR 1- SR 9) conducted at different stages of the test

Fig. 10. Comparison between the experimental (Hicher 2016) and the simulated nine undrained triaxial relaxation phases (SR 1- SR 9) along different stages of the undrained triaxial test with complex loading schemes presented in Fig. 9

Accepted manuscript doi:
10.1680/jgeot.23.00308

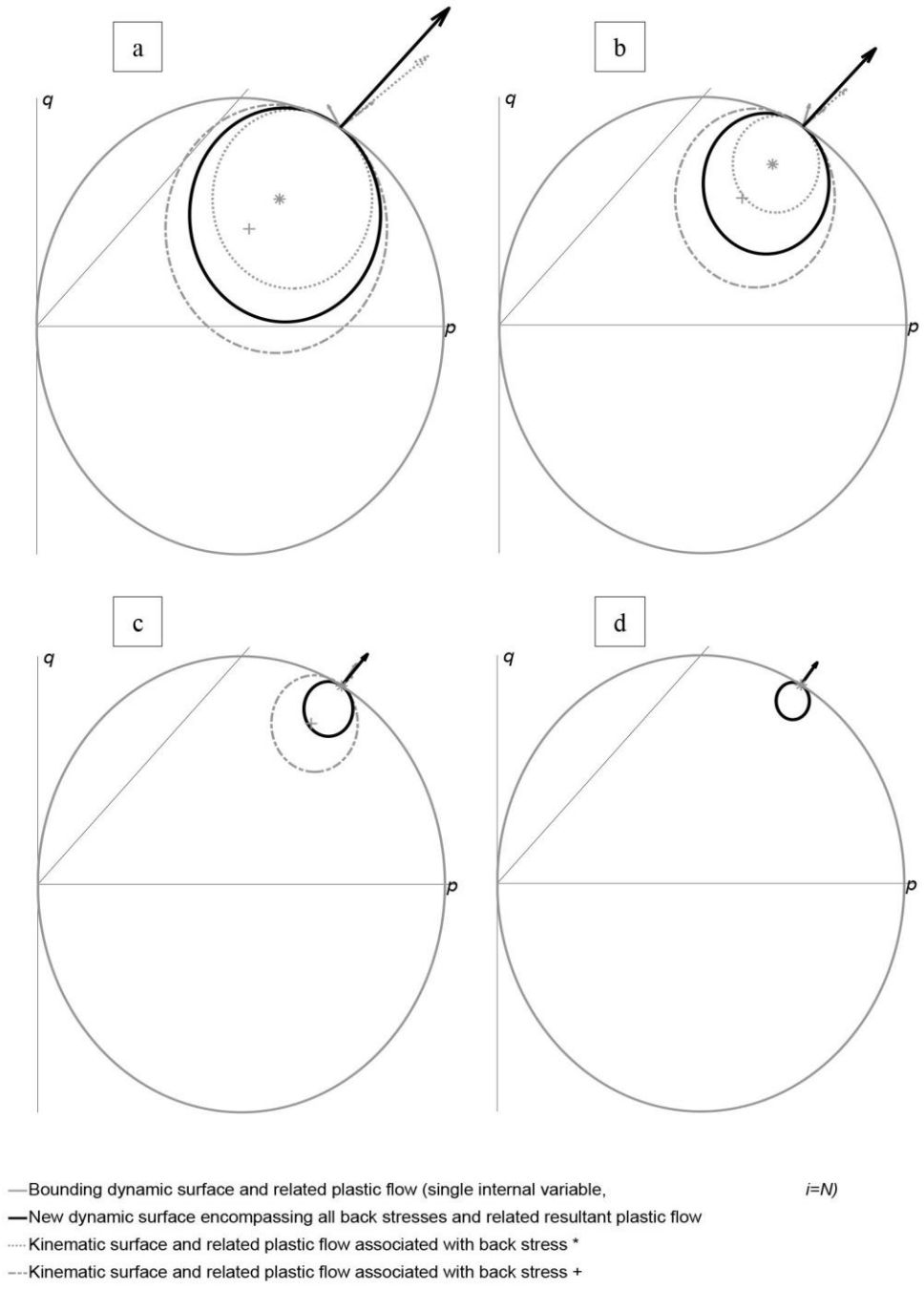

Fig_1

Accepted manuscript doi:
10.1680/jgeot.23.00308

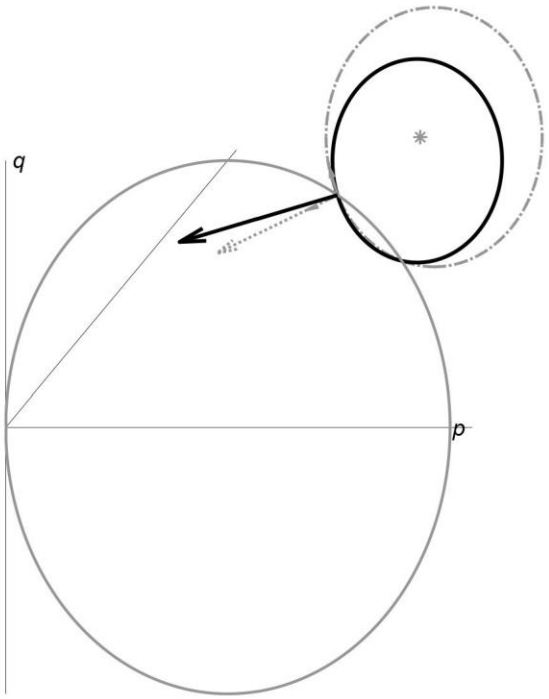

—Bounding dynamic surface and related plastic flow (single internal variable, *i=N)*
—New dynamic surface encompassing all back stresses and related resultant plastic flow
····Kinematic surface and related plastic flow associated with back stress *
----Kinematic surface and related plastic flow associated with back stress +

Fig_2

Accepted manuscript doi:
10.1680/jgeot.23.00308

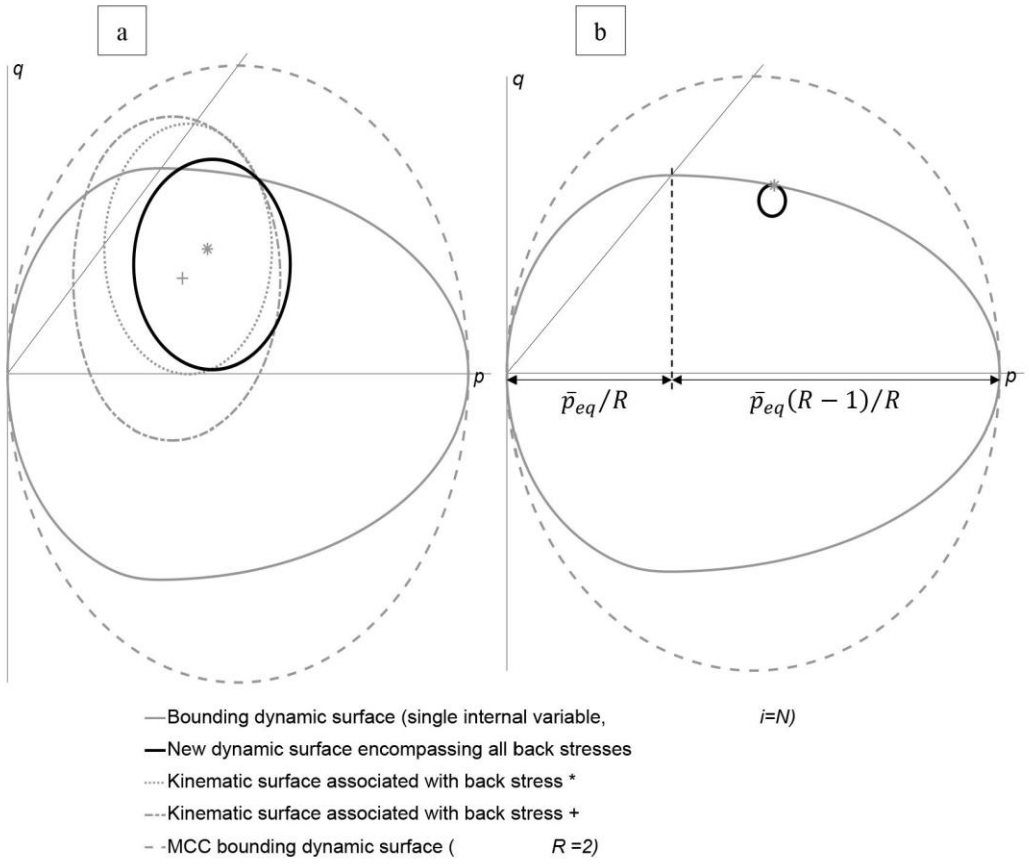

Fig_3

Accepted manuscript doi:
10.1680/jgeot.23.00308

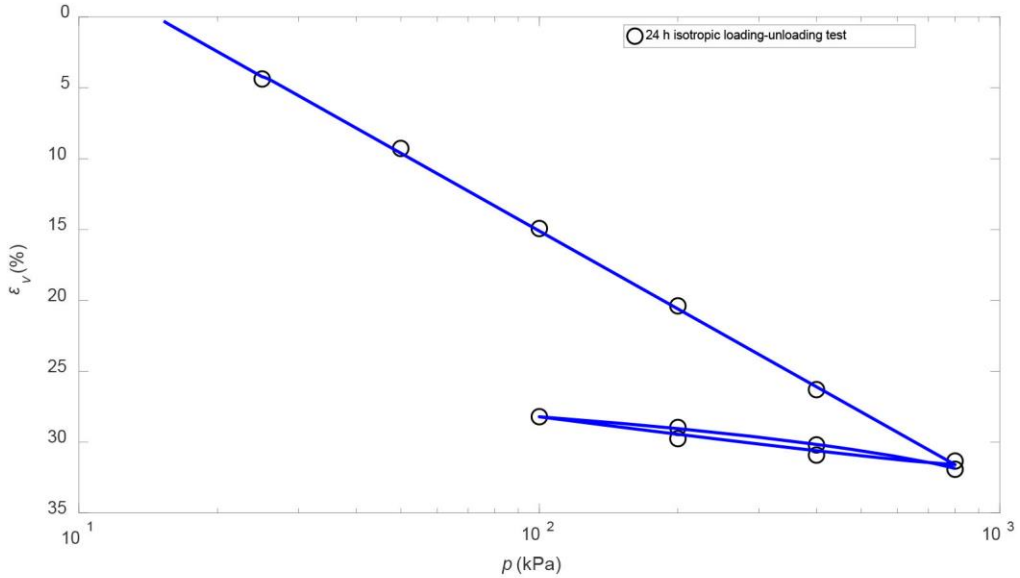

Fig_4

Accepted manuscript doi:
10.1680/jgeot.23.00308

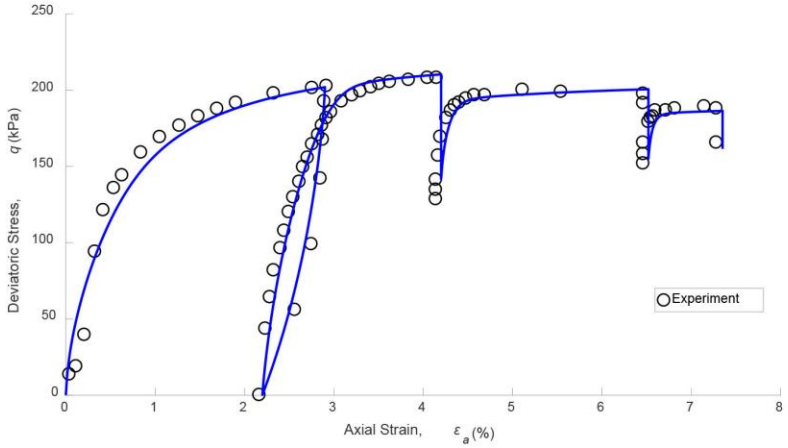

(a)

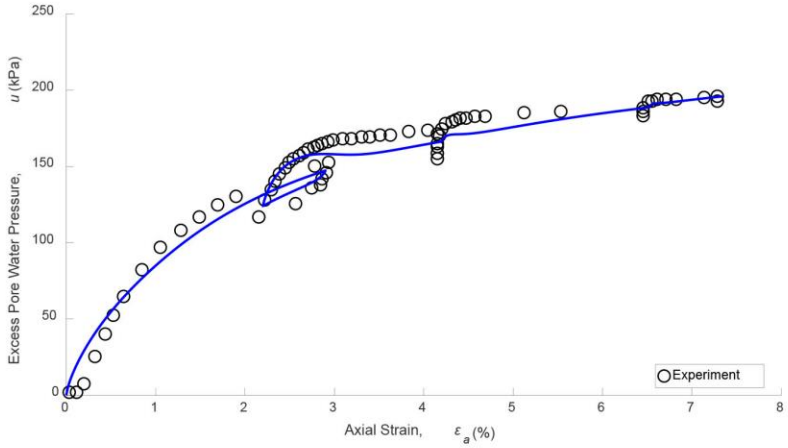

(b)

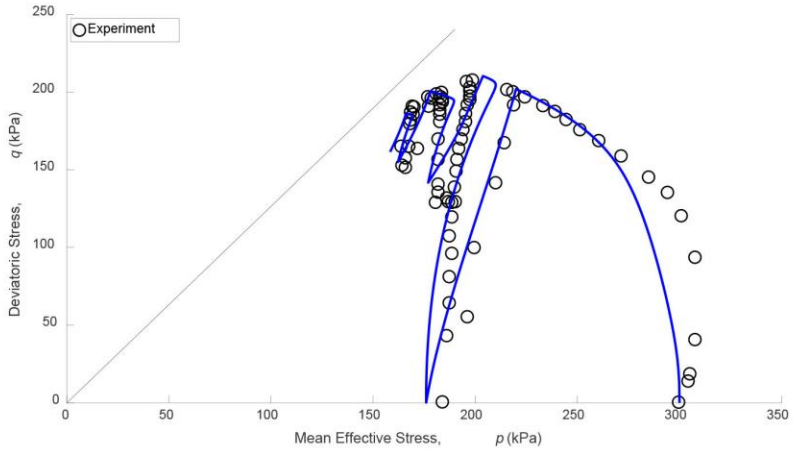

(c)

Fig_5

Accepted manuscript doi:
10.1680/jgeot.23.00308

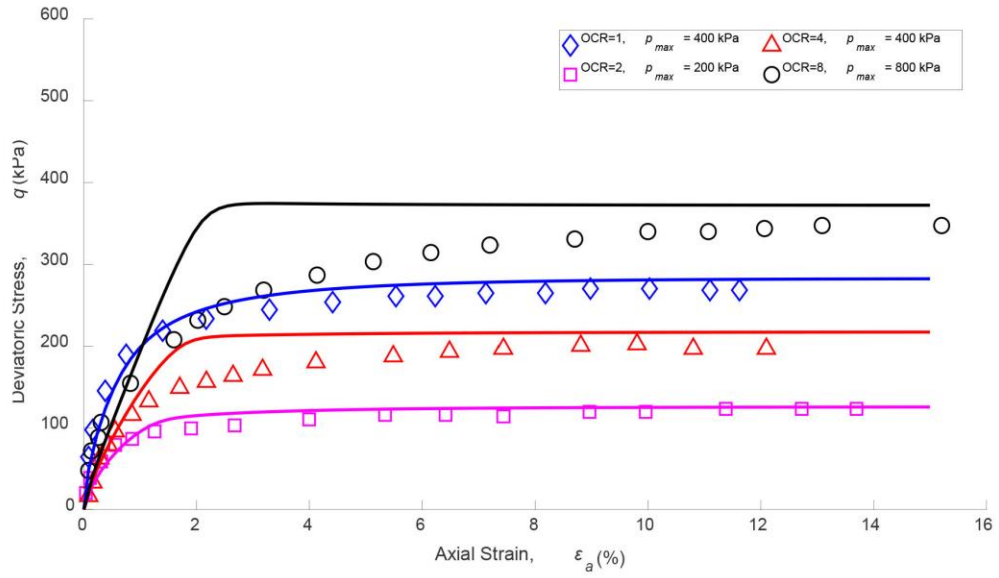

(a)

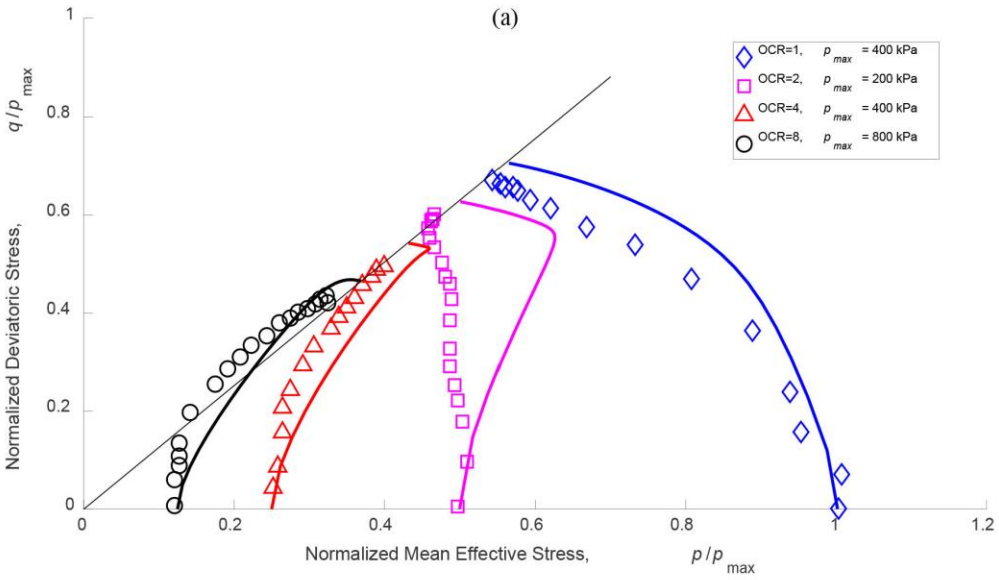

(b)

Fig_6

Accepted manuscript doi:
10.1680/jgeot.23.00308

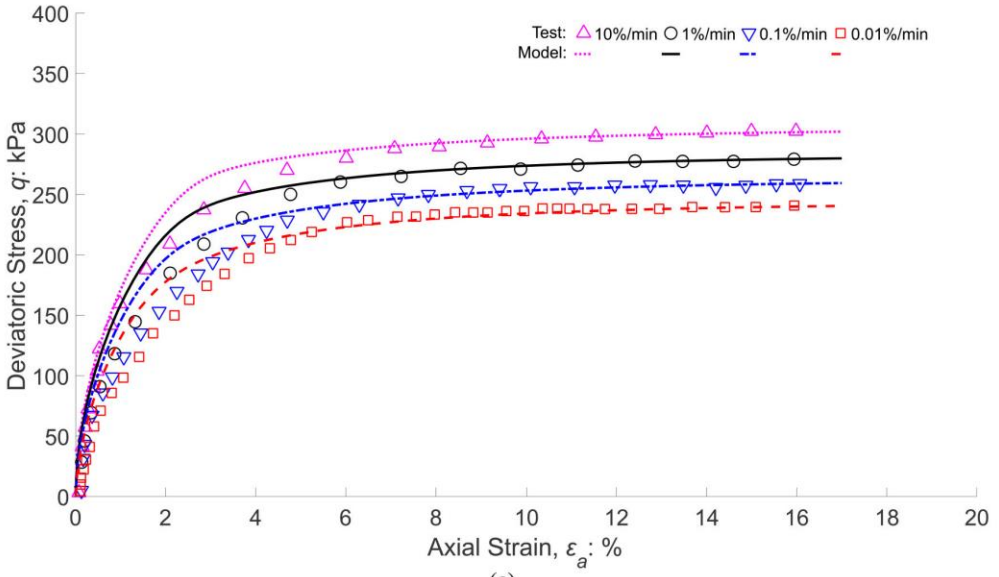

(a)

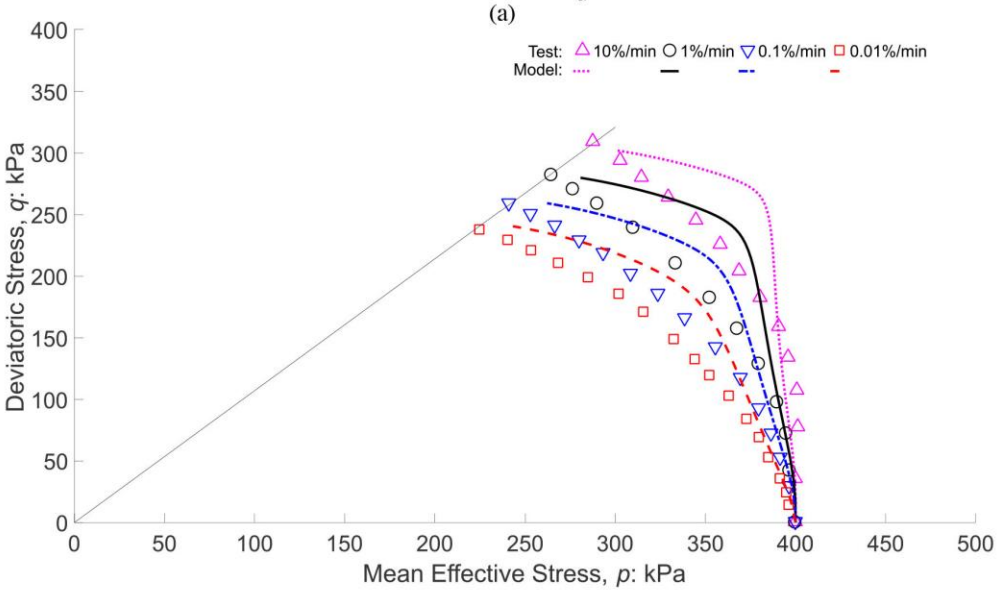

(b)

Fig_7

Accepted manuscript doi:
10.1680/jgeot.23.00308

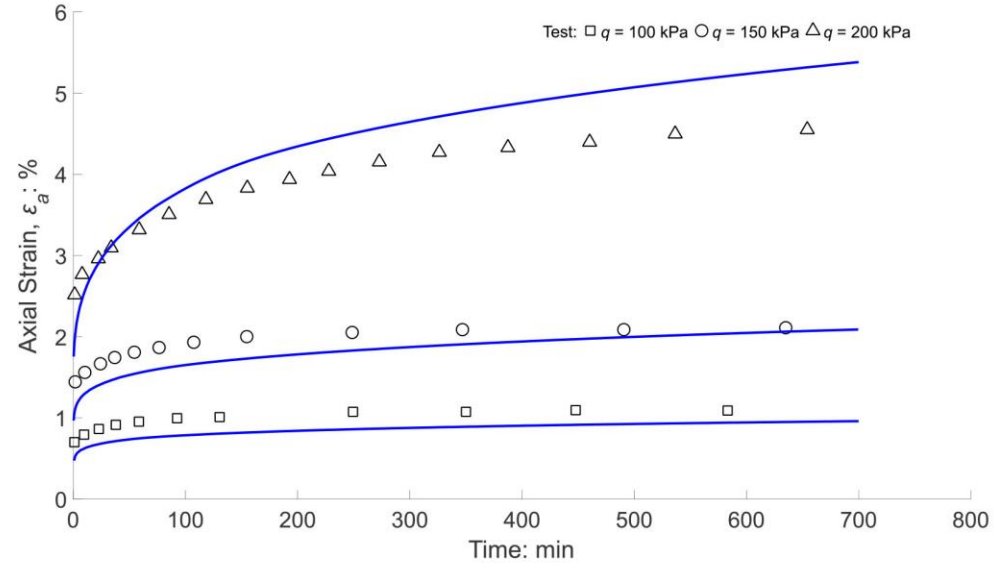

(a)

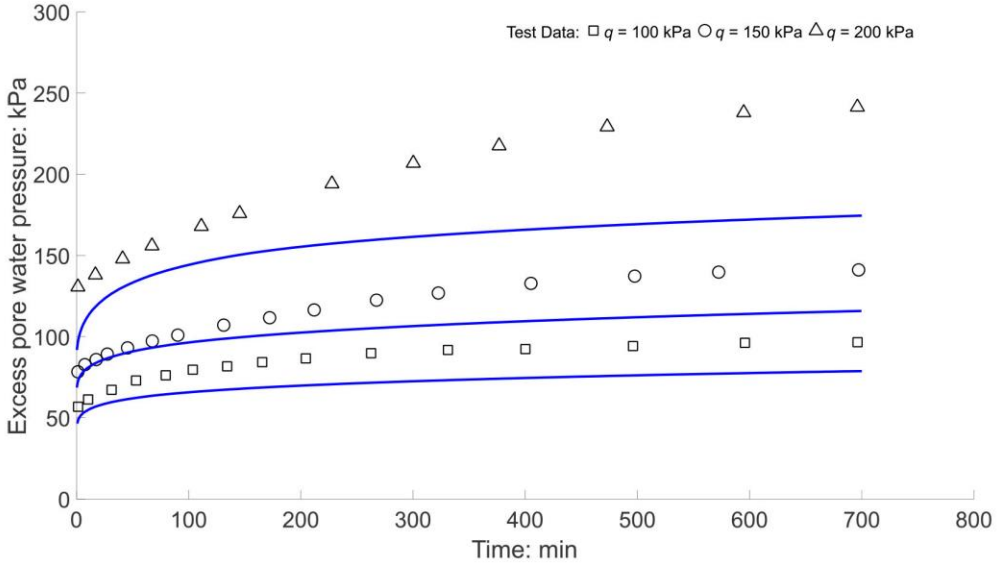

(b)

Fig_8

Accepted manuscript doi:
10.1680/jgeot.23.00308

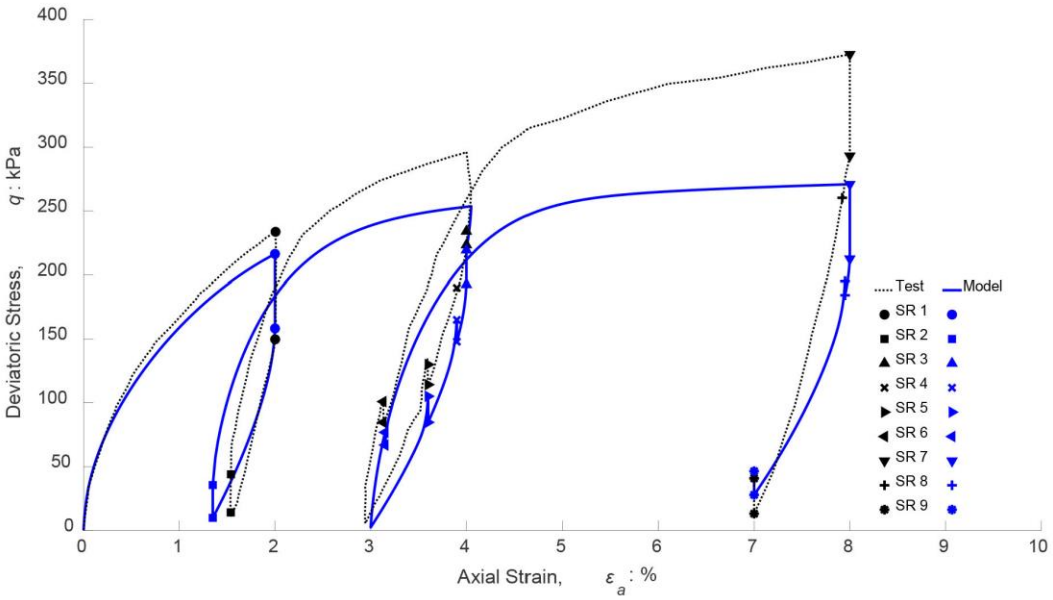

Fig_9

Accepted manuscript doi:
10.1680/jgeot.23.00308

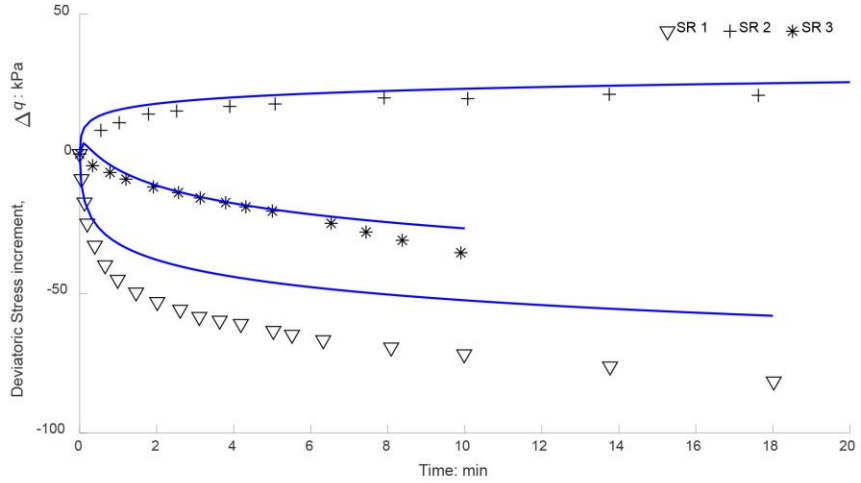

(a)

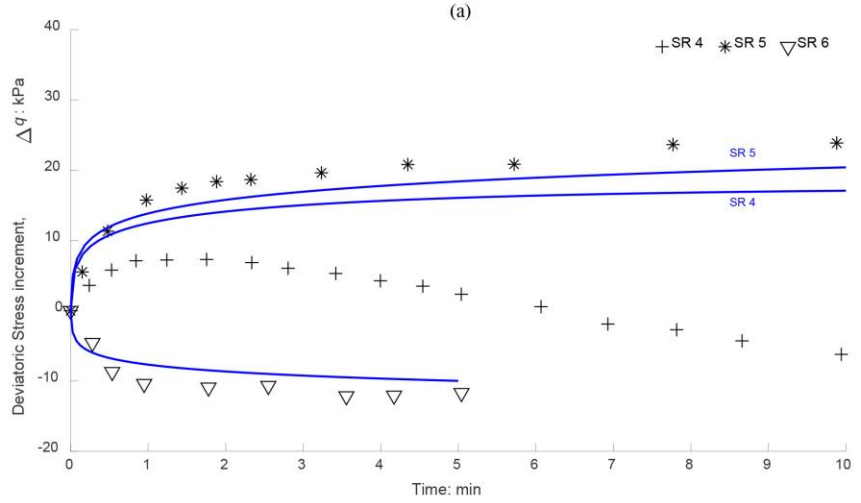

(b)

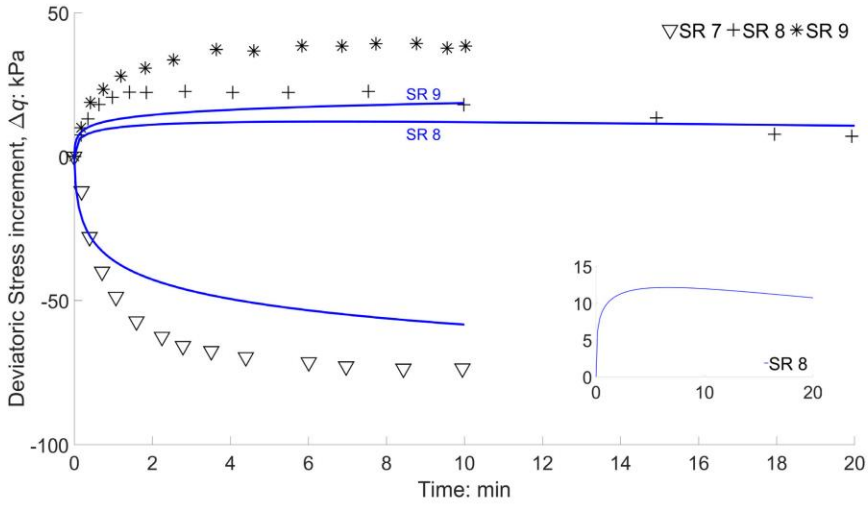

(c)

Fig_10